# The 30-year TAMSAT African rainfall climatology and time-series (TARCAT) dataset

AGU PUBLICATIONS

JGR

Journal of Geophysical Research: Atmospheres

RESEARCH ARTICLE
10.1002/2014JD021927

**Key Points:**
- Development of a satellite-based 30 year rainfall data set for Africa
- The data set has been designed to be temporally consistent
- The data set skillfully captures interannual and decadal variability

**Supporting Information:**
- Readme
- Figure S1
- Table S1

**Correspondence to:**
R. I. Maidment,
r.i.maidment@reading.ac.uk

**Citation:**
Maidment, R. I., D. Grimes, R. P. Allan, E. Tarnavsky, M. Stringer, T. Hewison, R. Roebeling, and E. Black (2014), The 30 year TAMSAT African Rainfall Climatology And Time series (TARCAT) data set, *J. Geophys. Res. Atmos.*, *119*, 10,619–10,644 doi:10.1002/2014JD021927.

Received 7 MAY 2014
Accepted 7 JUL 2014
Accepted article online 9 JUL 2014

The copyright line for this article was changed on 24 SEP 2014 after original online publication.



# The 30 year TAMSAT African Rainfall Climatology And Time series (TARCAT) data set

**Ross I. Maidment[1], David Grimes[1,2], Richard P. Allan[1], Elena Tarnavsky[1], Marc Stringer[1], Tim Hewison[3], Rob Roebeling[3], and Emily Black[1]**

[1]Department of Meteorology, University of Reading, Reading, UK, [2]Deceased 22 December 2011, [3]EUMETSAT, Darmstadt, Germany

**Abstract** African societies are dependent on rainfall for agricultural and other water-dependent activities, yet rainfall is extremely variable in both space and time and reoccurring water shocks, such as drought, can have considerable social and economic impacts. To help improve our knowledge of the rainfall climate, we have constructed a 30 year (1983–2012), temporally consistent rainfall data set for Africa known as TARCAT (Tropical Applications of Meteorology using SATellite and ground-based observations (TAMSAT) African Rainfall Climatology And Time series) using archived Meteosat thermal infrared imagery, calibrated against rain gauge records collated from numerous African agencies. TARCAT has been produced at 10 day (dekad) scale at a spatial resolution of 0.0375°. An intercomparison of TARCAT from 1983 to 2010 with six long-term precipitation data sets indicates that TARCAT replicates the spatial and seasonal rainfall patterns and interannual variability well, with correlation coefficients of 0.85 and 0.70 with the Climate Research Unit and Global Precipitation Climatology Centre gridded-gauge analyses respectively in the interannual variability of the Africa-wide mean monthly rainfall. The design of the algorithm for drought monitoring leads to TARCAT underestimating the Africa-wide mean annual rainfall on average by $-0.37\ \mathrm{mm\ d^{-1}}$ (21%) compared to other data sets. As the TARCAT rainfall estimates are historically calibrated across large climatically homogeneous regions, the data can provide users with robust estimates of climate related risk, even in regions where gauge records are inconsistent in time.

## 1. Introduction

Climate change and variability present a global challenge, but it is the less developed regions, such as Africa, where the population is most vulnerable [*Washington et al.*, 2006]. The heavy reliance on rain-fed agriculture and other water-related activities has resulted in many livelihoods being highly susceptible to rainfall variability [*Benson and Clay*, 1998; *Cooper et al.*, 2008]. Serious social and economic impacts arise when rainfall characteristics such as amount, intensity, frequency, and timing (for example, onset and cessation of the rainy season) differ from normal conditions. Moreover, the observed anthropogenic global warming over the last century is well documented [*Trenberth et al.*, 2007], but its effect on rainfall is less clear, particularly at regional scales [e.g., *Hulme et al.*, 2001; *Fauchereau et al.*, 2003; *Intergovernmental Panel on Climate Change*, 2013]. In addition, confidence in future precipitation scenarios is currently subject to large uncertainties [*Christensen et al.*, 2007] and can only be assured if there is a comprehensive understanding of the processes controlling rainfall variability, made possible through reliable rainfall records. An accurate and reliable understanding of the recent and present rainfall climate over Africa is therefore paramount. However, knowledge of the rainfall climate over Africa is limited mainly by inadequate ground-based rain gauge observations and the difficulty of detecting changes in a parameter that is highly variable in both space and time.

The lack or complete absence of surface observations has led to alternative, indirect methods of estimating rainfall becoming increasingly important for Africa. Rainfall estimates using satellite-based algorithms [e.g., *Xie and Arkin*, 1997; *Grimes et al.*, 1999; *Huffman et al.*, 2009; *Bergès et al.*, 2010; *Novella and Thiaw*, 2013] capable of providing full spatial coverage, have been shown to perform well over many parts of Africa, including West Africa [e.g., *Laurent et al.*, 1998; *Grimes et al.*, 1999; *Nicholson et al.*, 2003a, 2003b; *Roca et al.*, 2010; *Jobard et al.*, 2011], central and eastern Africa [e.g., *Dinku et al.*, 2007, 2008; *Maidment et al.*, 2013] and southern Africa [e.g., *Thorne et al.*, 2001; *Dinku et al.*, 2008; *Thiemig et al.*, 2012]. Satellite-based products typically exploit a combination of data from thermal infrared (TIR) and passive microwave (PMW) observations, as well as gauge observations. Since each of these data types has its own strengths, such as accuracy at a point

**Table 1.** Overview of Widely Used Rain Gauge and Satellite Rainfall Data Sets Providing Coverage for Africa, Including TARCAT

| Name | Data Input[b] | Spatial Resolution | Temporal Resolution | Spatial Coverage | Start Date | Primary Function[c] | Reference |
|---|---|---|---|---|---|---|---|
| GHCN | gauge | station | daily, monthly | global | 19th Century | climate | *Menne et al.* [2012] |
| CRU[a] | gauge | 0.5° | monthly | global | 1901 | climate | *Harris et al.* [2014] |
| GPCC First Guess | gauge | 1.0° | monthly | global | 2005 | climate | *Becker et al.* [2013] and *Schneider et al.* [2014] |
| GPCC monitoring product | gauge | 1.0°, 2.5° | monthly | global | 2007 | climate | *Becker et al.* [2013] and *Schneider et al.* [2014] |
| GPCC Full Data Reanalysis[a] | gauge | 0.5°, 1.0°, 2.5° | monthly | global | 1901 (end 2010) | climate | *Becker et al.* [2013] and *Schneider et al.* [2014] |
| GPCC VASClimo | gauge | 0.5°, 1.0°, 2.5° | monthly | global | 1951 (end 2000) | climate | *Becker et al.* [2013] and *Schneider et al.* [2014] |
| PREC/L[a] | gauge | 0.5°, 1.0°, 2.5° | monthly | global | 1948 | climate | *Chen and Xie* [2002] |
| University of Delaware | gauge | 0.5° | monthly | global | 1900 | climate | *Legates and Willmott* [1990] |
| GPCP-1DD | TIR, PMW, gauge | 1° | daily | global | 1996 | weather | *Huffman et al.* [2001] |
| GPI | TIR | 2.5° | monthly | 40°N–40°S | 1986 | climate | *Arkin and Meisner* [1987] |
| GPCP[a] | TIR, PMW, gauge | 2.5° | pentad, monthly | global | 1979 | climate | *Huffman et al.* [2009] |
| RFE | TIR, PMW, gauge | 0.1° | daily | 40°N–40°S, 20°W–55°E | 1995 | weather | *Herman et al.* [1997] |
| ARC[a] | TIR, gauge | 0.1° | daily | 40°N–40°S, 20°W–55°E | 1983 | climate | *Novella and Thiaw* [2013] |
| TRMM 3B42[a] | TIR, VIS, PMW, radar, gauge | 0.25° | 3 hourly, daily | 50°N–50°S, 0°–360°E | 1997 | weather | *Huffman et al.* [2007] |
| TRMM 3B43 | TIR, VIS, PMW, radar, gauge | 0.25° | monthly | 50°N–50°S, 0°–360°E | 1997 | climate | *Kummerow et al.* [2000] |
| CMORPH | TIR, PMW | 0.07° | 30 min | 60°N–60°S | 2002 | weather | *Joyce et al.* [2004] |
| PERSIANN | TIR, PMW | 0.25° | 6 hourly | 60°N–60°S | 2000 | weather | *Hsu and Sorooshian* [2008] |
| CMAP[a] | TIR, PMW, gauge, model | 2.5° | pentad, monthly | global | 1979 | climate | *Xie and Arkin* [1997] |
| EPSAT-SG | TIR, PMW, radar, gauge | 0.0375° | 15 min | Africa | 2004 | weather | *Bergès et al.* [2010] |
| MPE | TIR, PMW | 0.0375° | 15 min | Africa and Europe | 2007 | weather | *Heinemann and Gärtner* [2012] |
| KNMI-PPP | TIR, VIS, NIR | 0.0375° | 15 min (daytime) | Africa and Europe | 2004 | weather | *Roebeling et al.* [2012] |
| TARCAT[a] | TIR, gauge | 0.0375° | dekadal | Africa | 1983 | climate | - |

[a]Data sets which are described in further detail in section 2 and used in the intercomparison study in section 4.
[b]TIR = thermal infrared, NIR = near infrared, PMW = passive microwave, VIS = visible.
[c]The primary function gives the intended use of the data set, although some data sets may have interchangeable use. Data sets designated as *climate* refer to those products suited for climate applications, such as climate research and long-term monitoring analysis, while data sets designated *weather* refer to those products aimed at weather analysis, such as event-scale rain rates and rainfall coverage.

(rain gauge) and full spatial coverage (TIR imagery from geostationary platforms), combining each of these data types is often carried out to create an optimal product.

As satellite data archives now extend more than 30 years, such records potentially provide a powerful tool for assessing the rainfall climate. Numerous satellite-based rainfall products providing estimates for Africa exist, some of which are summarized in Table 1. Of these products, those that are considered temporally consistent, a necessity for reliably tracking year-to-year changes in rainfall, only cover short time periods (typically less than 15 years). Longer-term data products that are not calibrated against gauge data, such as the TIR Geostationary Operational Environmental Satellite (GOES) Precipitation Index (GPI) product [*Arkin and Meisner*, 1987; *Huffman et al*., 1997; *Joyce and Arkin*, 1997], may be subject to time-varying biases due to changing satellite data inputs that could introduce spurious artifacts. Satellite data sets that ingest contemporaneous gauge data help to minimize these biases and are highly valuable and generally reliable where sufficient gauge information is used. But the decline in gauge observations across Africa in recent decades [*Janowiak*, 1988; *Willmott et al*., 1994; *Nicholson*, 2001] and erratic reporting rates of Global Telecommunication System (GTS) stations [*Washington et al*., 2006] may introduce further temporal inconsistencies, particularly in data-sparse regions where sampling errors are likely to be greater. For example, it has been suggested by *Yin and Gruber* [2010] that the cause of a spurious downward trend in rainfall over the Congo River Basin in the Global Precipitation Climatology Project (GPCP) version 2.1

[*Adleret al*., 2003; *Huffman et al*., 2009] was partially a result of very few gauges used in the analyses. *Wan et al*. [2013] who investigated the effect of the spatial and temporal coverage of global in situ gauge observations on the estimation of mean, variance, and trend in rainfall also demonstrated that over data-sparse regions such as Africa, large sampling errors in total precipitation and trend magnitude may exist. These issues mean that, although there are clear advantages to including ground-based rainfall measurements in satellite-based products, the method by which gauge measurements are incorporated is likely to impact the rainfall estimates. The methodology used for combining satellite imagery with gauge measurements, furthermore, may affect the suitability of the data product for assessing long-term trends. This is especially the case in regions where the gauge records are sparse and temporally inconsistent.

In this paper, we report on the development of a new gridded 30 year TIR-based precipitation data set called the Tropical Applications of Meteorology using SATellite and ground-based observations (TAMSAT) African Rainfall Climatology And Time series (TARCAT). The TARCAT data set (1983–2012) is based on the TAMSAT rainfall estimation algorithm [*Dugdale et al*., 1991; *Milford et al*., 1996; *Grimes et al*., 1999] that was originally developed over West Africa during the 1980s and has recently been extended to all parts of Africa for all months [*Tarnavsky et al*., 2014]. TAMSAT's primary objective has been to provide historic and near real-time rainfall estimates for drought monitoring over sub-Saharan Africa. The method depends on two inputs, namely TIR imagery and gauge observations. The high temporal sampling (15 or 30 min) provided by Meteosat TIR imagery is suitable for capturing the rapid development of convective storms that is not possible from TIR and PMW sensors on low Earth-orbiting platforms. Unlike the majority of combined satellite-gauge algorithms (see Table 1), in creating TARCAT, gauge information is only used to generate climatological calibrations that vary spatially and monthly to reflect the geographical and temporal variations in the average rainfall climate across Africa. An important prerequisite of the TAMSAT system is that these empirically derived calibration parameters do not change from year to year, eliminating the need for contemporaneous gauge data. The temporal variation in rainfall, inferred from the TARCAT data set, is therefore largely unaffected by gauge sampling biases. Rainfall estimates are then obtained by applying the predetermined calibration parameters to cold cloud duration (CCD) fields calculated from TIR data (see section 3.3), on the assumption that cold clouds produce the majority of rainfall across Africa. This TAMSAT technique has been shown to perform well over many parts of Africa when compared to gauge data, and despite the relative simplicity of the TAMSAT algorithm has comparable skill to other satellite-based products [*Laurent et al*., 1998; *Thorne et al*., 2001; *Dinku et al*., 2007; *Chadwick et al*., 2010; *Jobard et al*., 2011; *Maidment et al*., 2013]. This skill underlines the suitability of TIR-based algorithms over Africa and highlights the importance of adjusting the algorithm to local climatic conditions [*Dugdale et al*., 1991; *Todd et al*., 1995, 1999; *Dybkjær*, 2003; *Chadwick et al*., 2010]. Because the TAMSAT method has good skill, we have not modified the original algorithm for the development of TARCAT, for example, by using more complex techniques of estimating rainfall using TIR brightness temperatures [e.g., *Kidd et al*., 2003].

TIR-based algorithms, such as TAMSAT, are well suited for Africa because of the overwhelming dominance of deep convective systems that are responsible for most of the precipitation across the continent [*Mohr and Zipser*, 1996; *Mohr et al*., 1999; *Nesbitt et al*., 2000; *Mathon et al*., 2002]. These convective systems range from isolated cumulonimbus cells that may last for a couple of hours to large-scale organized mesoscale convective systems that may persist for several days. TIR-based algorithms are successful over much of Africa because there is a strong relationship between the cold cloud tops (or cloud top temperature derived indices such as CCD) of these systems and precipitation. Such cold cloud tops are easily distinguishable from warmer nonprecipitating shallower clouds and the land surface below and hence provide a useful indicator of rainfall occurrence. Because these rain-bearing convective systems are associated with the seasonal migration of the Intertropical Convergence Zone (ITCZ), the resulting annual cycle in rainfall is often consistent from year to year at any one location making it permissible to use a climatology-based calibration approach, as used in generating TARCAT.

In order to meet the requirements of drought monitoring, TAMSAT dekad rainfall estimates and subsequent anomalies (with respect to the 1983–2012 average) are created every 10 days (accessible from http://www.met.reading.ac.uk/~tamsat/data) at a spatial resolution of 0.0375° (approximately 4 km) at nadir, consistent with TARCAT. While the retrieval error can be considerably large at this resolution compared to areal averages [*Grimes et al*., 2003], provision of the data at this scale allows users to aggregate the data to suitable scales for specific applications. While TARCAT is a 30 year data set, the near real-time TAMSAT estimates generated since January 2013 use the same calibrations used in TARCAT

and are therefore consistent with the long-term data set. The remainder of this paper details the steps taken to construct the TARCAT data set and compares TARCAT with some widely used long-term satellite and gauge rainfall data sets.

## 2. Overview of Rainfall Data Sets

An overview of some widely used observation based (satellite and gauge) data sets that provide rainfall estimates for Africa is given in Table 1 while those data sets used in this paper are described here. The majority of the satellite products give global or near-global coverage, but few are tailored solely for Africa. *Jobard et al*. [2011] demonstrated that over West Africa, the data sets tailored for Africa, including TAMSAT, generally have greater skill than global products. Numerical weather prediction reanalysis model products are not discussed here as it is well documented that over Africa modeled rainfall is less accurate than satellite-based products, especially at subcontinental scales [e.g., *Lim and Ho*, 2000; *Poccard et al*., 2000; *Funk and Verdin*, 2003; *Diro et al*., 2009; *Maidment et al*., 2013]. This is because forecast and general circulation models, which operate at relatively course resolutions (typically 50 km or greater), are not able to explicitly resolve the small-scale processes associated with tropical convection and precipitation. Instead, they rely on parameterizations that approximate precipitation processes across a model grid square, such as the cloud microphysics and determining how much rainfall is generated. However, uncertainties in these approximations and model physics can lead to large errors in the estimated precipitation [*Pope et al*., 2000; *Yang and Slingo*, 2001; *Allan et al*., 2007; *Flato et al*., 2013; *Pearson et al*., 2014]. Moreover, the inability of these models to simulate small-scale precipitation accurately highlights the advantage of the high spatial resolution of the TARCAT data set in capturing the spatial variability of convective rainfall across Africa.

### 2.1. Rain Gauge Observations

Gauge-only products can be categorized into either point or gridded data sets. Such data sets are, in some cases, later merged with satellite-only rainfall estimates to improve the accuracy of the satellite estimates. There are several archives that maintain original gauge records, for example, the Global Historical Climate Network (GHCN) [*Menne et al*., 2012]. Such data sets are an amalgamation of records from numerous sources, including records from national meteorological services and Surface Synoptic Observations reports via the GTS network. These data sets can provide long-term station records and are excellent for climate analysis at their individual point locations. However, such records are rarely complete and can be susceptible to time-dependent biases such as changes in the device and the surrounding environment [*Sevruk*, 1982; *Legates and Willmott*, 1990].

More often used are gridded-gauge products that include the Climate Research Unit (CRU) precipitation data set [*Mitchell and Jones*, 2005; *Harris et al*., 2014], those from the Global Precipitation Climatology Centre (GPCC) [*Becker et al*., 2013; *Schneider et al*., 2014] and the National Oceanographic and Atmospheric Administration (NOAA) PRECipitation REConstruction over Land (PREC/L) [*Chen and Xie*, 2002]. Like GHCN, these gridded data sets combine observations from multiple sources. Because of the longevity of these data sets (see Table 1), they are best suited for climate-based analysis, including evaluation of climate models. Such products generally perform well in places where the density of the gauge network is high, for example, in Europe and North America [*Schneider et al*., 2014]. However, in much of Africa where the gauge network is sparse and unevenly distributed, conversion from point to areal averages may be subject to large representativeness errors [*Flitcroft et al*., 1989; *Rudolf et al*., 1994; *Willmott et al*., 1994; *Xie and Arkin*, 1995]. The high spatial variability associated with convective rainfall exacerbates this problem.

While much effort is made to ensure consistency of gridded-gauge data sets, the station density is rarely consistent over time. In the current GPCC Full Data Reanalysis gauge analysis [*Becker et al*., 2013; *Schneider et al*., 2014], the total number of gauges used across Africa has decreased by approximately 80% from 1983 to 2010 (see discussion in section 3.5). It is possible that due to data latency, additional records may become available for the most recent years. Nonetheless, such a reduction may increase sampling errors of gridded products, particularly in data-sparse regions, increasing uncertainty in trends derived over such regions [e.g., *Wan et al*., 2013]. This has potential significance as many combined satellite-gauge products depend on such gridded-gauge analyses.

### 2.2. Satellite-Based Observations

The monthly GPCP precipitation analysis [*Adler et al*., 2003; *Huffman et al*., 2009] provides global coverage since 1979 at 2.5° resolution and is particularly useful for climate research, including model evaluation. The estimation algorithm uses GPI rainfall estimates adjusted against PMW observations (since 1987) over the Tropics using the method described by *Adler et al*. [1994] and augmented by sounding observations at higher latitudes. Finally, the combined satellite estimates are adjusted to gauge measurements where available (the latest GPCP version 2.2 uses the GPCC's Full Data Reanalysis product). It should be noted that none of the satellite inputs span the entire period (from 1979 to the present), and therefore, changes in the rainfall estimation scheme has taken place (details: ftp://precip.gsfc.nasa.gov/pub/gpcp-v2.2/doc/V2.2_doc.pdf). *Lau and Wu* [2007] suggest that the decrease in GPCP rainfall over Equatorial Africa since 1987 may be related to the inclusion of PMW data.

The NOAA Climate Prediction Center African Rainfall Estimation Algorithm (NOAA-RFE) produces rainfall estimates in near real-time to assist drought monitoring across sub-Saharan Africa. Estimates are created by linearly combining TIR (GPI estimates) and PMW rainfall estimates using predetermined weighting coefficients before merging with GTS gauge records (full description: http://www.cpc.ncep.noaa.gov/products/fews/RFE2.0_tech.pdf). Merging of the satellite estimates and GTS gauge data follows the method of *Reynolds* [1988] whereby an attempt is made to remove the bias in the satellite estimates using the gauge data, while retaining the spatial distribution of precipitation given by the satellite estimates. As of January 2001, a major change in the product occurred with NOAA-RFE version 1.0 [*Herman et al*., 1997] being replaced by NOAA-RFE version 2.0. NOAA-RFE version 1.0 only used TIR (i.e., GPI) and GTS observations while NOAA-RFE version 2.0 utilizes two types of PMW data as described above. A daily climatological version of NOAA-RFE known as the African Rainfall Climatology (ARC) is available from 1983 to the present which uses the NOAA-RFE version 1.0 algorithm [*Love et al*., 2004; *Novella and Thiaw*, 2013]. Because ARC has a relatively long time series, it has functions in both climate research and long-term monitoring applications.

The Climate Prediction Center (CPC) Merged Analysis of Precipitation (CMAP) [*Xie and Arkin*, 1997] provides rainfall estimates from 1979 at 2.5° resolution and is similar to GPCP and NOAA-RFE in that it utilizes TIR, PMW, and gauge records but also incorporates model reanalysis outputs. While CMAP provides a long time series, which is important for climate analysis, the data set is known to suffer from temporal discontinuities due to changes in calibration methods and inclusion of new data types during the record [*Yin et al*., 2004; *Lau and Wu*, 2007].

The Tropical Rainfall Measuring Mission (TRMM) is aimed at improving observations of precipitation across the Tropics [*Kummerow et al*., 2000; *Huffman et al*., 2007]. The TRMM satellite is equipped with a precipitation radar (PR), the TRMM microwave imager, and a visible-infrared scanner from which different TRMM precipitation products are generated. The PR is perhaps the best satellite instrument to date at capturing precipitation features such as intensity, distribution, and type, but temporal sampling is low, with up to two overpasses daily for a given location. The most widely used outputs are the TRMM Multisatellite Precipitation Analysis (TMPA) 3-hourly (3B42) and monthly (3B43) products. These precipitation estimates, classed as level 3 products, use TRMM level 1 and 2 products to calibrate and adjust merged-TIR imagery from geostationary and polar-orbiting platforms and are then adjusted against GPCC gauge information where possible to provide near-global coverage at a spatial resolution of 0.25°. While studies have shown these TRMM products perform well over Africa [*Nicholson et al*., 2003b; *Dinku et al*., 2007; *Jobard et al*., 2011], estimates are only available since 1997 which is arguably too short a period for inference of long-term climate trends. TRMM products, in particular 3B42, are perhaps best suited for event-based applications, such as estimates of rain rates and rainfall coverage.

## 3. Development of the TARCAT Data Set

The 30 years of TAMSAT rainfall estimates that constitute the TARCAT data set required Meteosat TIR imagery to generate the CCD fields and gauge records for calibrating the CCD fields. The Meteosat TIR data set starting in 1981 was obtained from the European Organisation for the Exploitation of Meteorological Satellites (EUMETSAT) archives. Incomplete records and unavailable sensor calibration information meant that the first 2 years (1981 and 1982) were not retained. Corrupt files in the remaining data were identified and removed manually. Data from January 1983 to June 2006 originated from the Meteosat First Generation (MFG) satellites (Meteosat 2–7), while subsequent data came from Meteosat Second Generation (MSG) satellites (Meteosat 8–9). As of January 2013, real-time data are received from Meteosat-10. The central wavelengths of the window channels used are 11.5 μm and 10.8 μm for MFG and MSG, respectively. The gauge archive used to generate the

regional monthly calibration parameters comprised of around 4300 stations (see Appendix A) providing over 350 000 records of 10 day rainfall totals from 1983 to 2010, the majority of which have been obtained from numerous African National Meteorological and Hydrological Centres during workshops since the early 1990s.

The TARCAT data set has been created by firstly generating CCD fields, which are used in conjunction with the gauge records to derive the spatially and temporally varying climatological calibration parameters, and secondly, applying the TAMSAT algorithm and derived calibration parameters to the CCD fields from 1983 to 2012. The following subsections detail the steps and quality control procedures taken during the data set development.

### 3.1. Meteosat Calibration and Conversion to Brightness Temperature

The methodology for converting raw radiometric counts to brightness temperature is longstanding [e.g., *van de Berg et al*., 1995; *Picon et al*., 2003; *Novella and Thiaw*, 2013]. Adopting the notation of *Picon et al*. [2003], the MFG relationship between radiance and radiometric counts is given by equation (1);

$$R = \alpha(C - C_0) \tag{1}$$

where $R$ is radiance, $\alpha$ is the calibration coefficient, $C$ is the observed digital Meteosat radiometric count, and $C_0$ is the background space count. The calibration coefficient and space count values were obtained from the EUMETSAT web site (http://www.eumetsat.int/website/home/Data/Products/Calibration/MFGCalibration/index.html). An analytical approximation of Planck's law (equation (2)) was then applied to convert the radiances to brightness temperature $T$.

$$T = \frac{B}{(\ln R - A)} \tag{2}$$

The nonlinear coefficients $A$ and $B$ were determined by EUMETSAT using radiance and brightness temperature lookup reference tables for each satellite and were sourced online (ftp://gerb.oma.be/Documents/imager_dictionary.pdf) and from historic calibration reports issued by EUMETSAT. The conversion from radiometric counts to radiance for MSG data is identical to MFG data (equation (1)), but the radiance-brightness temperature relationship is given by a three parametric formulation of the inverse Planck function [*Govaerts et al*., 2001, Equation (3)];

$$T = \frac{1}{\alpha}\left[\frac{c_2 v_C}{\ln\left(1 + v_C^3 \frac{C_1}{R}\right)} - \beta\right] \tag{3}$$

where $v_c$ is the representative wave number (inverse of the channel wavelength) and $\alpha$, $\beta$, $C_1$, and $C_2$ are coefficients that are radiometer dependent (available from: http://www.eumetsat.int/website/home/Data/Products/Calibration/MSGCalibration/index.html). Due to changes in Meteosat data in May 2008, including radiance definition (see previous reference for details), an error up to −0.35 K is expected for MSG data from July 2006 to May 2008. However, the resultant error is very small (~2%) for TAMSAT rainfall estimates (see section 3.3). During the conversion process, all images were projected onto a latitude-longitude grid and parallax corrections applied. A caveat of geostationary imagery is the change in ground resolution (and thus the cloud-fraction observed) with zenith angle; however, most of the area where rainfall is estimated is generally within the middle of the satellite disk view where this has least effect.

### 3.2. Meteosat Brightness Temperature Record

An analysis of the full Meteosat TIR time series is extremely valuable for the climate community, particularly since it is used in many climate data sets [e.g., *Schiffer and Rossow*, 1985; *Rossow and Schiffer*, 1999], including precipitation data sets. However, exploiting the Meteosat TIR archive for climate analysis presents its own challenges. Using imagery from eight different satellites over the 30 year period (see Figures 1a–1d (top)) can introduce artificial temporal discontinuities, either during the life time of a single instrument or from a change of instrument. Such instrument-dependent biases may result in misleading trends in rainfall. These discontinuities have different causes, such as differences in the spectral response functions of the channel, spectral degradation over time, or spectral shifts over time. In addition, the space agencies operating the satellites regularly adapt the calibration techniques employed. All the above reasons motivated the initiative taken by the World Meteorological Organization to establish the Global Space-based Inter-Calibration System, which aims to ensure consistent calibration and intercalibration of operational meteorological

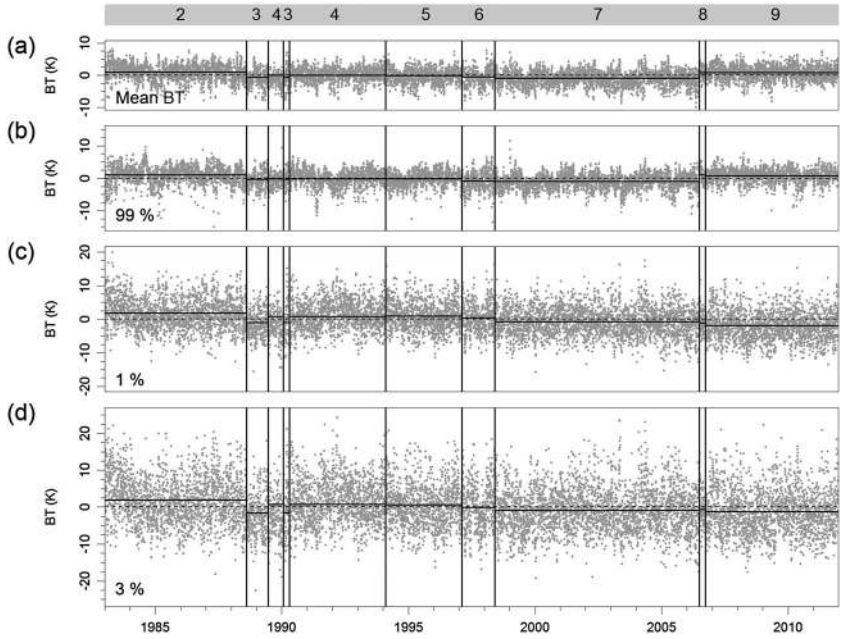


**Figure 1.** Deseasonalized time series of Meteosat brightness temperature (BT) daily statistics (grey dots) over the domain (20°S–20°N, 15°W–40°E) for (a) mean brightness temperature, (b) 99th percentile, (c) 1st percentile, and (d) 3rd percentile. The data were deseasonalized by subtracting the daily climatology (computed over all instruments from 1983 to 2011 period) from each daily value for each statistic. The vertical lines indicate the satellite changes. The horizontal solid lines give the mean brightness temperature for each satellite. There were occasional periods, typically only lasting a couple of days, when the operational satellite was replaced with a preexisting Meteosat satellite. These are not illustrated here but are included in the calculation of the mean brightness temperature for each satellite. (top) A reference for the Meteosat satellite in operation during each period over which the mean brightness temperature has been computed. Full details of the operational history of the Meteosat satellites can be found on the EUMETSAT website (http://www.eumetsat.int/website/home/Satellites/PastSatellites/index.html).

satellite instruments [*Goldberg et al*., 2011]. While significant biases in the Meteosat water vapor channel exist [*Picon et al*., 2003], no such studies have yet been conducted on the full Meteosat TIR archive. Because a temporally consistent satellite record is essential for the long-term reliability of TARCAT, particularly as no contemporaneous gauge adjustment to the satellite estimates is incorporated, it was necessary to carefully evaluate the Meteosat TIR archive for any time-dependent biases.

An assessment was carried out by extracting daily brightness temperature statistics from the TIR archive over a domain covering most of the African continent where deep tropical convection occurs (20°S–20°N, 15°W–40°E). The statistics considered were the spatial mean and pixel value corresponding to the 1st (cold scene) and 99th (warm scene) percentiles. The latter two were included to represent the full range of scene temperatures and to determine if biases were temperature dependent. The coldest and warmest pixels were also considered but were not found to provide sufficiently robust statistics. Here the 1st percentile is representative of the cloud top temperature of cumulonimbus or cirrus clouds, which are thought to offer a stable calibration target [e.g., *Doelling et al*., 2004; *Zelinka and Hartmann*, 2011], while the 99th percentile is sensitive to land surface temperature and emissivity. The final statistic considered over this domain was the 3rd percentile, which corresponds, on average to 228 K. This is the midpoint of the cloud top temperature range that the TAMSAT method considers (see Appendix A) and is a useful measure relevant to the TAMSAT algorithm.

The deseasonalized time evolution of these statistics from 1983 to 2011 is presented in Figure 1. The mean brightness temperature for each Meteosat satellite for each statistic considered is superimposed onto the time series (see Table 2 and Table S1 in the supporting information). The mean brightness temperature provides a useful measure to assess any temporal discontinuities associated with a change in satellite, particularly where the time period considered is relatively short.

It is evident from Figure 1 that satellite-dependent biases do exist. For the warm scene (Figure 1b), sudden changes occur with the transition to Meteosat-3, to Meteosat-7, and to Meteosat-8/9. Since a typical satellite view

**Table 2.** Brightness Temperature Summary Statistics (Mean, Standard Deviation (SD) and Standard Error (SE)) for Each Meteosat Satellite for Each of the Statistics Presented in Figure 1[a]

| | Mean BT (K) | | | 99th Percentile (K) | | | 1st Percentile (K) | | | 3rd Percentile (K) | | |
|---|---|---|---|---|---|---|---|---|---|---|---|---|
| Satellite | Mean | SD | SE | Mean | SD | SE | Mean | SD | SE | Mean | SD | SE |
| 2 | 282.93 | 2.65 | 0.06 | 316.11 | 3.91 | 0.09 | 213.29 | 4.88 | 0.11 | 228.81 | 6.77 | 0.15 |
| 3 | 281.06 | 2.81 | 0.14 | 315.40 | 4.24 | 0.21 | 209.73 | 4.56 | 0.23 | 224.25 | 6.57 | 0.33 |
| 4 | 281.88 | 2.29 | 0.06 | 314.50 | 3.70 | 0.09 | 212.57 | 4.70 | 0.12 | 228.13 | 6.56 | 0.17 |
| 5 | 281.78 | 2.37 | 0.07 | 314.84 | 3.43 | 0.10 | 212.51 | 4.75 | 0.14 | 227.56 | 6.58 | 0.20 |
| 6 | 281.44 | 2.90 | 0.13 | 315.01 | 3.88 | 0.18 | 211.28 | 4.84 | 0.22 | 226.22 | 6.83 | 0.31 |
| 7 | 280.95 | 2.45 | 0.05 | 314.04 | 3.98 | 0.07 | 210.82 | 4.58 | 0.08 | 226.23 | 6.48 | 0.12 |
| 8 | 282.46 | 2.16 | 0.19 | 314.43 | 3.09 | 0.27 | 211.10 | 4.73 | 0.42 | 227.13 | 6.24 | 0.55 |
| 9 | 282.70 | 2.26 | 0.05 | 315.74 | 3.46 | 0.08 | 209.69 | 4.90 | 0.11 | 225.75 | 6.72 | 0.16 |

[a]The deseasonalized statistics are available in the supporting information.

over the domain considered is generally dominated by warm scenes, a similar scenario exists for the mean brightness temperature (Figure 1a). An apparent cold bias exists for Meteosat-3 as well as Meteosat-7, although the latter is well documented [*Hewison*, 2013; *Hewison and Muller*, 2013; *Hewison et al*., 2013]. For cold scenes, the 1st (Figure 1c) and 3rd (Figure 1d) percentiles both indicate a possible cold (wet) bias for Meteosat-3 in the order of 2–3 K, but there is no indication that a considerable bias exists for any other satellites, including Meteosat-7. However, there is large variability for cold scenes compared to the warmer scenes making it more difficult to detect biases.

It is plausible that relatively cold Meteosat-3 3rd percentile brightness temperature may be explained by increased rainfall and cold cloud relating to La Niña conditions [*Nicholson and Selato*, 2000]. Similarly, a warmer 3rd percentile during 1983/1984 (evident in Figure 1a) coincided with drier than average conditions across the continent [*Lamb and Peppler*, 1992; *Hoerling et al*., 2006]. Percentiles corresponding to 243 K, 233 K, 223 K, and 213 K (temperature thresholds used by the TAMSAT method) yielded similar results to the 3rd percentile (not shown). Although not investigated in this study, observing differences between satellites can be due to factors such as changes in the spectral response function, spatial resolution, radiometric noise, quantization of the instruments, and satellite drift. Efforts are currently underway by EUMETSAT to assess the aforementioned factors [*Roebeling et al*., 2013]. These results indicate that although different satellites have contributed to the Meteosat record, the calibration information supplied by EUMETSAT yields a stable TIR satellite record adequate for generating TARCAT. There is, however, a gradual but statistically significant (at the 99% confidence level using a Mann-Kendall trend test) decreasing trend in the satellite-mean brightness temperature for the 1st and 3rd percentile (see Figure 1 and Tables 2 and S1), suggesting an increase in cold cloud from 1983 to 2011 (discussed in section 4.3). Despite the apparent stability of the full TIR data set, the Meteosat record was not originally intended for climate research, and therefore, potentially large TIR calibration uncertainties may mask weak rainfall signals. Biases in rainfall estimates due to the change from MFG to MSG imagery were also investigated but were found to be significantly smaller compared to other sources of error discussed in subsequent sections.

### 3.3. TAMSAT Algorithm and Algorithm Sensitivity

The TAMSAT algorithm [*Dugdale et al*., 1991; *Milford et al*., 1996; *Grimes et al*., 1999] is an example of a cloud-indexing technique. Using Meteosat TIR imagery, the length of time over a 10 day period where the cloud top temperature is colder than a predetermined optimum temperature threshold ($T_t$) is calculated, known as CCD. CCD is used as the proxy for rainfall. Provided sufficient temporal and/or spatial averaging, the 10 day CCD total is then linearly related to rainfall $R$;

$$R = \begin{cases} a_0 + a_1 \mathrm{CCD} & \mathrm{CCD} > 0 \\ 0 & \mathrm{CCD} = 0 \end{cases} \quad (4)$$

where $a_0$ and $a_1$ are the regression calibration coefficients. These coefficients and the optimum temperature threshold are derived locally (known as calibration zones [e.g., *Thorne et al*., 2001]) on a monthly basis using the extensive archive of gauge records (see Appendix A for details on the derivation of the calibration parameters). It is assumed that zero CCD corresponds to zero rainfall. During the CCD calculation, if there is a temporal gap between two temperature measurements, half the period is taken to be at the temperature of the earlier time and the other half at the temperature of the later time to form a step-change. Hence, for a regular MSG

**Table 3.** Sensitivity of TAMSAT Rainfall Estimates to Systematic Changes in the Satellite Brightness Temperature[a]

| | Temperature Change (K) | | | | |
|---|---|---|---|---|---|
| | 1 | 2 | 3 | 4 | 5 |
| MAE (mm/d) | 0.13 | 0.27 | 0.41 | 0.54 | 0.67 |
| MAPE (%) | 6.52 | 13.47 | 20.37 | 26.79 | 33.38 |

[a]The reported error statistics (mean absolute error (MAE) and mean absolute percentage error (MAPE)) are derived by perturbing the Africa-wide calibration temperature thresholds by ±1 to 5 K to simulate an apparent systematic bias in Meteosat brightness temperature and computing the overall difference between the perturbed rainfall estimate and the unperturbed rainfall estimate. Study based on all rainfall dekads in 2002; 72 dekads were used to compute each statistic.

15 min gap between temperature measurements, a temperature measurement below the threshold temperature contributes 7.5 min before and 7.5 min after its time, a total of 15 min.

To test the significance a possible satellite instrument bias might have on TAMSAT rainfall estimates, temperature thresholds used in the monthly operational calibrations were perturbed (by ±1 to 5 K) to simulate an apparent change in the satellite brightness temperature. Rainfall estimates using the adjusted temperature thresholds were then compared to rainfall estimates using the operational temperature thresholds.

The mean errors (see Appendix B for formulae) computed for all dekads in 2002 are given in Table 3 (and in Figure S1a). Warmer (cooler) Meteosat TIR retrievals result in less (more) cold cloud detected, leading to a dry (wet) bias. On average, a perturbation of 1 K results in an offset in rainfall of ±0.13 mm $d^{-1}$ (6.5%). In the case of a possible 3 K cold bias for Meteosat-3, a wet bias of 0.41 mm $d^{-1}$ (20.4%) may be expected. Such biases are systematic across the satellite disk view, although larger errors are expected for colder temperature thresholds (see Figure S1b). For example, a perturbation of 3 K at a threshold of 213 K gives an error of 0.57 mm $d^{-1}$ (28.0%) compared to 0.31 mm $d^{-1}$ (14.6%) at 243 K. The increased sensitivity at colder thresholds is explained by fewer occurrences of cold cloud exceeding 213 K compared to 243 K. These findings indicate that the TAMSAT algorithm is quite insensitive to small changes in cloud top temperature due to the indirect use of Meteosat radiances in rainfall estimation.

### 3.4. Recovery of Missing Rainfall Dekads

Due to missing satellite imagery, particularly during the 1980s and early 1990s (Figure 2), a complete set of dekadal rainfall estimates from 1983 to the present has not been possible. By using the standard TAMSAT approach which allows gaps in TIR data of up to 3 h, rainfall estimates for 207 dekads would not be generated. However, by employing two procedures, we recovered 179 (86%) of these missing dekads. If up to 6 h of TIR data are missing, daily CCD fields are estimated as described in section 3.3 using data from time slots on either side of the missing data interval. A longer gap (>6 h) increases the chance of missing a storm, and thus, 6 h is the largest acceptable gap; if more than 6 h of TIR data are missing, the daily CCD field is not estimated. At the end of a dekad, if up to two daily CCD fields are missing, they are replaced with daily mean CCD for the dekad. We have quantified the likely errors associated with data recovery (see Appendix C for details); these errors therefore apply to the 179 recovered dekads, less than 20% of the total (existing and recovered) dekads that constitute the TARCAT data set. The estimated root-mean-square error (RMSE) did not exceed 0.64 mm $d^{-1}$ (17.3%) at 0.5° resolution, which is much smaller than the typical errors in TAMSAT rainfall estimates reported in validation studies [cf. *Laurent et al.*, 1998; *Dinku et al.*, 2007; *Chadwick et al.*, 2010; *Maidment et al.*, 2013]. The TAMSAT webpage and header of each file provides users with quality flags where recovery procedures have been used.

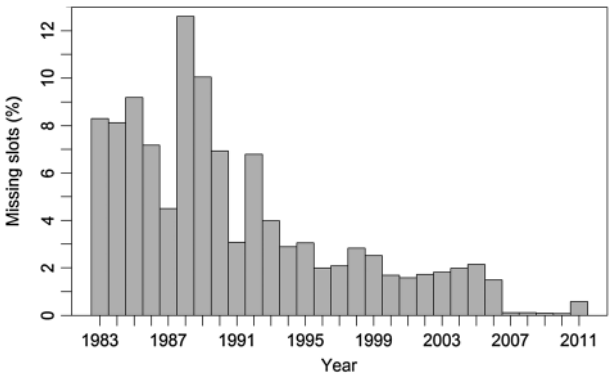


**Figure 2.** The annual percentage of missing TIR time slots calculated as the percentage difference between existing slots (i.e., images obtained from the Meteosat archive) and all possible slots.

### 3.5. Temporal Stability of the TAMSAT Calibration Parameters

The primary objective in generating TARCAT is to create a temporally consistent rainfall data set. For this purpose, a one-off calibration was imposed, which varies for each month and calibration zone, but remains constant over all years. Hence, any interannual variability in rainfall can be accounted for by fluctuations in the amount of cold cloud rather than a continually changing calibration. It is reasonable to assume that a fixed monthly calibration may not accurately reflect submonthly changes in precipitation systems and that the same rainfall-CCD relationship may not occur at the same time every year. While it is nontrivial accounting for such changes without additional information (e.g., gauge or PMW), TAMSAT validation studies have demonstrated that using a single monthly calibration applied over several years yields reliable rainfall estimates [*Laurent et al*., 1998; *Thorne et al*., 2001; *Dinku et al*., 2007; *Chadwick et al*., 2010; *Jobard et al*., 2011; *Maidment et al*., 2013].

The calibrations are derived using all available gauge observations from 1983 to 2010. For many parts of Africa, the gauge records used do not span this full time period, and therefore, the calibration may be biased to the gauge observation period. The resulting calibration can be considered to be a climatological calibration representing the mean rain-CCD relationship over the years where gauge observations were available. Since *Dugdale et al*. [1991] demonstrated that over the Sahel, the calibration can vary from year to year depending on whether it is a dry or wet year (using data from 1986 to 1989), a single climatological calibration may underestimate the year-to-year variance in rainfall. However, *Dugdale et al*. [1991] indicated that the change in calibration is not important for rainfall totals less than 2 mm $d^{-1}$. Furthermore, *Dugdale et al*. [1991] based the "wet" calibration on a period (1988–1989) that was considerably wetter than average [*Nicholson and Selato*, 2000]. It is therefore important to assess whether a single calibration is representative of the rain-CCD relationship across all 30 years over Africa. Furthermore, if a prolonged shift in rainfall regime has occurred, this may alter the rain-CCD relationship, particularly in a changing climate where precipitation processes are unlikely to remain constant.

We have tested the temporal stability of the calibration using an empirical approach by validating TARCAT with a reference data subset over southern Africa, to detect any periods where a systematic bias may exist (Figure 3). The reference data set used was the GPCC Full Data Reanalysis v6.0 gridded-gauge analysis [*Becker et al*., 2013; *Schneider et al*., 2014] (hereinafter referred to as GPCC-FDR; see Table 1). GPCC-FDR was used as it overlaps with most of the TARCAT years and over southern Africa, the gauge density remained comparatively high for most of the period (Figure 3d) suggesting that the resulting gridded GPCC-FDR rainfall estimates are unlikely to suffer from any large sampling errors. While the gauge data used in GPCC-FDR is likely to overlap with that used in the TAMSAT calibration, the data sets are fundamentally different as it is the satellite observations that drive the year-to-year changes in TARCAT. It is clear that TARCAT is able to reproduce the rainfall amounts given by GPCC-FDR reasonably well (Figures 3a and 3f). The two data sets disagree by less than 0.6 mm $d^{-1}$ (monthly rainfall) 90% of the time and 0.85 mm $d^{-1}$ on average the other 10% of the time. The monthly anomaly (Figure 3b) and annual rainfall (Figure 3c) time evolutions provide no evidence of inhomogeneity or trends (in the monthly anomaly) indicating that the TAMSAT calibration over this region is acceptable from 1983 to 2010. Figure 3c also shows that TARCAT is able to track the interannual variability given by GPCC-FDR well ($r = 0.90$), although TARCAT is drier than GPCC-FDR (discussed in section 4.2). Figure 3e gives the number of gauges from the region used in the TAMSAT calibrations. Since the majority of these observations cover the 1990s with very little data from the 2000s and negligible data from 1980s, the good agreement between TARCAT and GPCP-FDR demonstrates that for this region, the calibration is not biased to the rainfall climate of the 1990s and can be applied to other time periods. The mean annual cycle is also given (Figure 3g) and shows that TARCAT is very similar to GPCC-FDR. A validation of rainfall estimates over Uganda by *Maidment et al*. [2013] demonstrated that the TAMSAT rainfall estimates calibrated using 1993–2000 gauge records performed well for the years from 2001 to 2005 indicating that at least for this region, a single calibration can perform well for other years independent of the calibration data set.

## 4. Evaluation of Rainfall Climatology and Interannual Variability

Here we present the mean rainfall climatology and interannual variability (1983–2010) depicted by the TARCAT data set and those of six long-term satellite precipitation and gridded-gauge data sets (described in section 2). The satellite data sets are GPCP v2.2 [*Adler et al*., 2003; *Huffman et al*., 2009], CMAP v1201 [*Xie and Arkin*, 1997] and ARC v2.0 [*Novella and Thiaw*, 2013; hereinafter ARC2]. The gauge data sets are CRU v3.10 [*Harris et al*., 2014], GPCC-FDR, and NOAA's PREC/L (updated January 2011) [*Chen and Xie*, 2002].

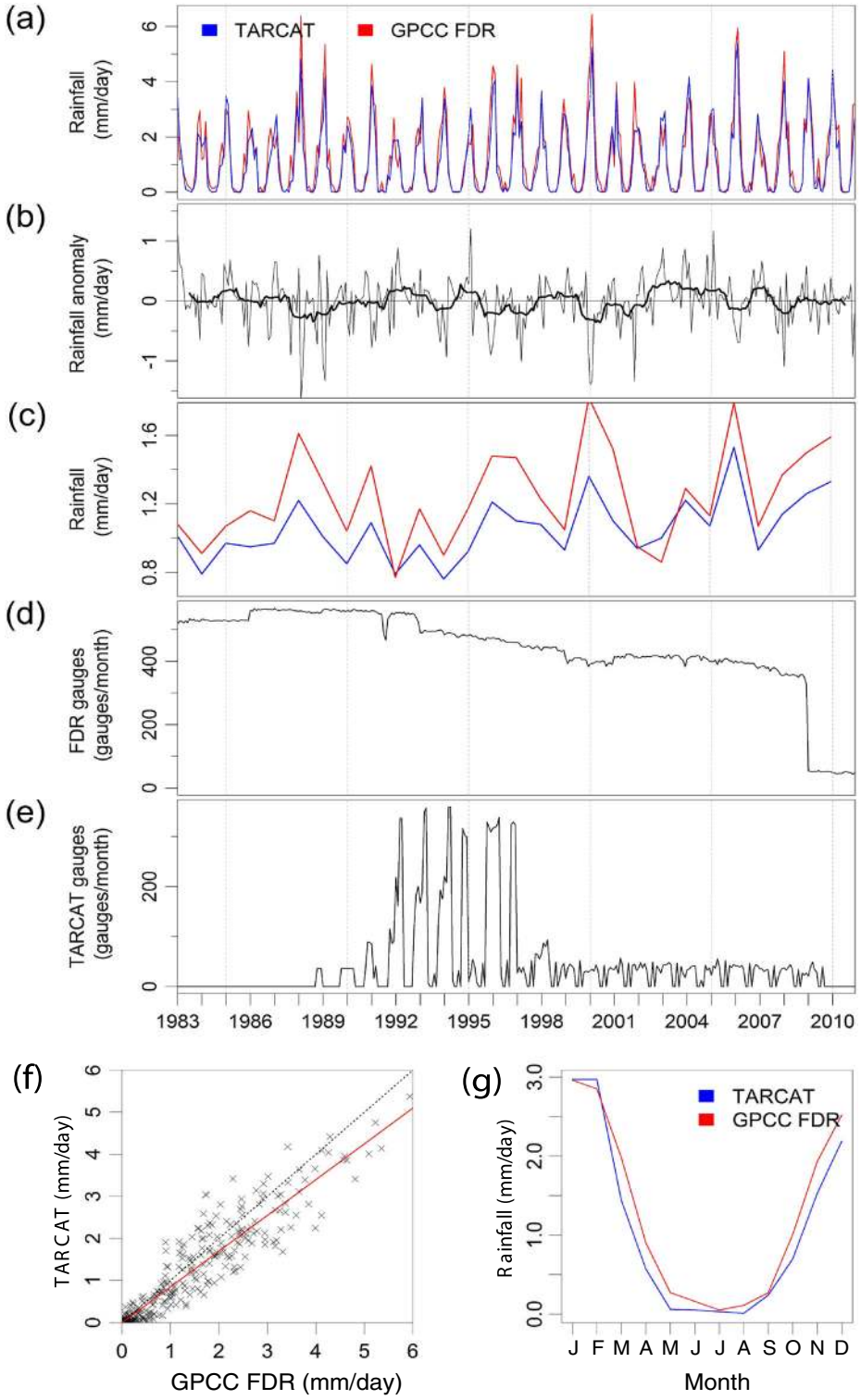


**Figure 3.** The time evolution of (a) TARCAT and GPCC Full Data Reanalysis monthly rainfall estimates averaged over the domain −28°S to −18°S, 22°E to 28°E (southern Africa), (b) the resulting anomaly computed as TARCAT-GPCC FDR (using deseasonalized values; annual running mean in bold line), (c) the annual rainfall estimates, (d) number of GPCC FDR rain gauges over the domain, and (e) the number of rain gauges over the domain used in the TAMSAT calibration. Using the same data, comparisons of (f) monthly rainfall estimates (dashed line denotes the one-to-one correspondence and red line denotes the linear regression best fit) and (g) mean monthly annual cycle.

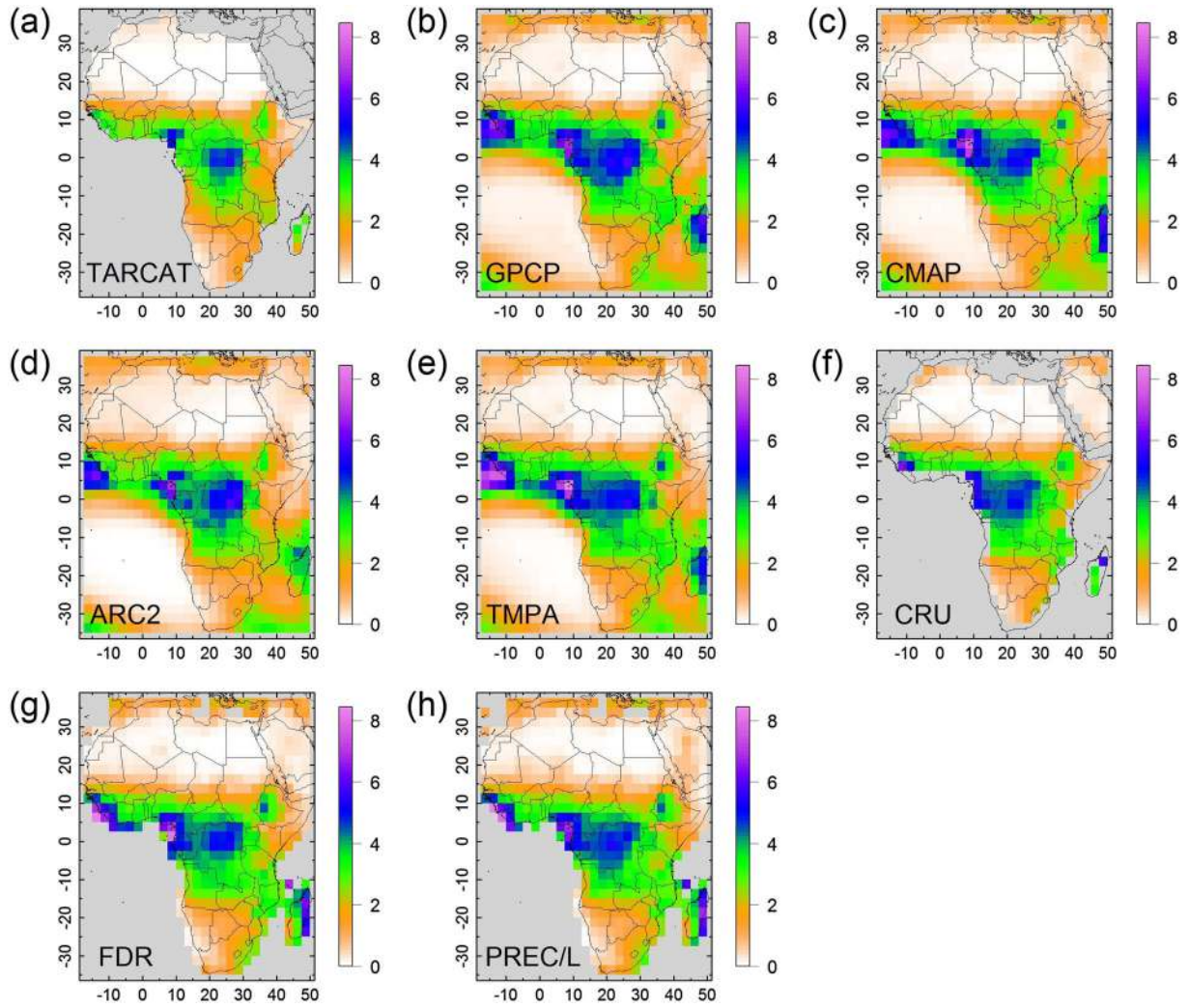


**Figure 4.** Spatial annual rainfall climatology (mm $d^{-1}$) over the period 1983 to 2010 for (a) TARCAT, (b) GPCP, (c) CMAP, (d) ARC2, (e) TMPA (using 1998–2010 estimates), (f) CRU, (g) GPCC-FDR, and (h) PREC/L at 2.5° resolution.

Three gauge data sets were chosen to highlight the variation in gauge data sets brought about by differences in sampling of gauge records and data set construction techniques.

All of these data sets (except ARC2) provide monthly mean rainfall at 2.5° resolution. ARC2 data (daily totals on a 0.1° grid) and TARCAT data (dekadal totals on a 0.0375° grid) were converted to monthly means on a regular 2.5° by 2.5° grid. To address the missing TARCAT dekads, we interpolated anomalies across each of the remaining 28 missing dekads and conducted an anomaly adjustment to the TARCAT climatology for the missing dekad.

TARCAT is the only satellite data set considered here that does not combine contemporaneous gauge data with the satellite estimates. The merging of gauge data into the other satellite products means that comparisons against GPCC-FDR, CRU, and PREC/L cannot be interpreted as independent validations. It is, moreover, to be expected that satellite products produced in this way would agree closely with gauge based data sets. In contrast, although TARCAT does include gauge data in its calibration, its year-to-year variability is purely based on the signal from satellite imagery. To some extent, therefore, the comparisons of TARCAT against the gauge-only data sets can be considered a validation.

### 4.1. Climatology

The spatial annual rainfall climatology for TARCAT and the other precipitation data sets is presented in Figure 4. Despite being only available since the late 1990s, the TMPA 3B42 v7.0 data set [*Kummerow et al.*, 2000; *Huffman*

**Table 4.** Africa-Wide Annual and Seasonal Mean Rainfall (Using Land-Only Values) From 1983 to 2010 (Units: mm $d^{-1}$)

| | Annual | DJF | MAM | JJA | SON |
|---|---|---|---|---|---|
| TARCAT | 1.37 | 1.37 | 1.33 | 1.43 | 1.36 |
| GPCP | 1.82 | 1.85 | 1.71 | 1.85 | 1.89 |
| CMAP | 1.69 | 1.68 | 1.59 | 1.77 | 1.73 |
| ARC2 | 1.64 | 1.72 | 1.59 | 1.53 | 1.74 |
| TMPA[a] | 1.82 | 1.83 | 1.67 | 1.88 | 1.89 |
| CRU | 1.73 | 1.69 | 1.64 | 1.79 | 1.80 |
| GPCC-FDR | 1.71 | 1.73 | 1.62 | 1.76 | 1.76 |
| PRECL | 1.75 | 1.72 | 1.68 | 1.80 | 1.79 |

[a]TMPA values computed from 1998 to 2010.

*et al*., 2007, 2010; hereinafter TMPA] has been included because of its wide use. The 3-hourly TMPA estimates were summed to monthly averages and regridded to 2.5° resolution, consistent with the remaining data sets. It can be seen that the rainfall distribution given by TARCAT is similar to other data sets, with rainfall maxima in the same regions, namely, Guinea coastal regions, Congo Basin, Ethiopian highlands, and Madagascar. However, it is noticeably drier than the other data sets, particularly along parts of the Guinea coast and northern Madagascar. The annual mean bias between TARCAT and the other data sets is $-0.37\,\mathrm{mm\,d^{-1}}$ (21%) and the seasonal mean biases are $-0.38\,\mathrm{mm\,d^{-1}}$ (22%), $-0.31\,\mathrm{mm\,d^{-1}}$ (17%), $-0.34\,\mathrm{mm\,d^{-1}}$ (23%), and $-0.44\,\mathrm{mm\,d^{-1}}$ (24%) for December, January, and February (DJF), March, April, and May (MAM), June, July, and August (JJA), and September, October, and November (SON), respectively (see Table 4). There is little to differentiate between the other data sets, but as was explained above, this is likely attributed to each of the data sets ingesting similar contemporaneous gauge data.

The mean monthly annual cycle of the eight data sets is shown in Figure 5. All data sets have been masked using identical land-only grids available in all data sets. TARCAT follows the same annual cycle given by the other data sets with peak rainfall in March and August. The TARCAT dry bias is clearly evident but is generally consistent throughout most months except the months of February, May, and November, which have larger biases. Regional analyses (not shown) show that the larger biases in February, May, and November occur only over the Congo Basin where very few gauges exist. Elsewhere, TARCAT is more consistent with the other data sets throughout all months. The other satellite-based data sets agree well with the seasonal pattern given by the gauge data sets in terms of magnitude and seasonality of rainfall. The exception is the dry bias of ARC2 during the boreal summer months which has been explained by a lack of GTS gauge records over West Africa [*Novella and Thiaw*, 2013].

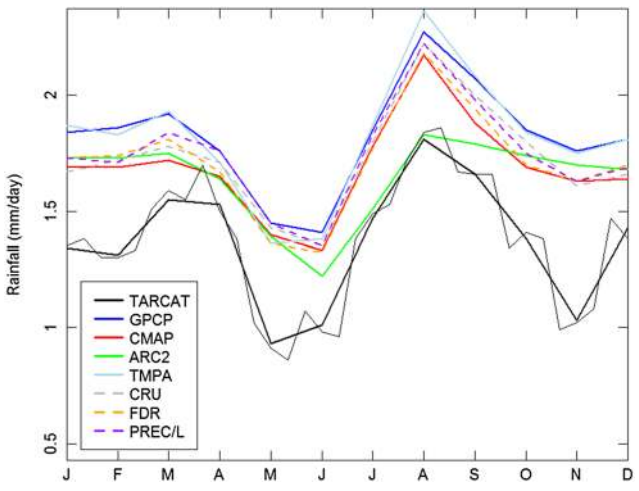


**Figure 5.** Africa-wide area-average monthly annual cycle of rainfall for TARCAT, GPCP, CMAP, ARC2, TMPA (using 1998–2010 estimates), CRU, GPCC-FDR, and PREC/L over 1983 to 2010 using land-values only. Solid lines represent satellite-based data sets while dashed lines represent gauge-only data sets. The thin solid black line denotes TARCAT dekadal values.

### 4.2. TARCAT Dry Bias

TIR-based products are known to underestimate high-intensity rainfall events [*Kidd and Huffman*, 2011; *Kidd and Levizzani*, 2011]; however, this alone would not lead to the ~20% dry bias observed. The bias can be explained by the approach used for calibrating the TAMSAT algorithm. Since TAMSAT is geared toward drought monitoring where accurately representing low rainfall amounts is given priority, the median rainfall for given CCD bins is chosen to regress against the midpoint for each CCD bin (see *Grimes et al*. [1999] and Appendix A for further calibration details). Because rainfall amounts are

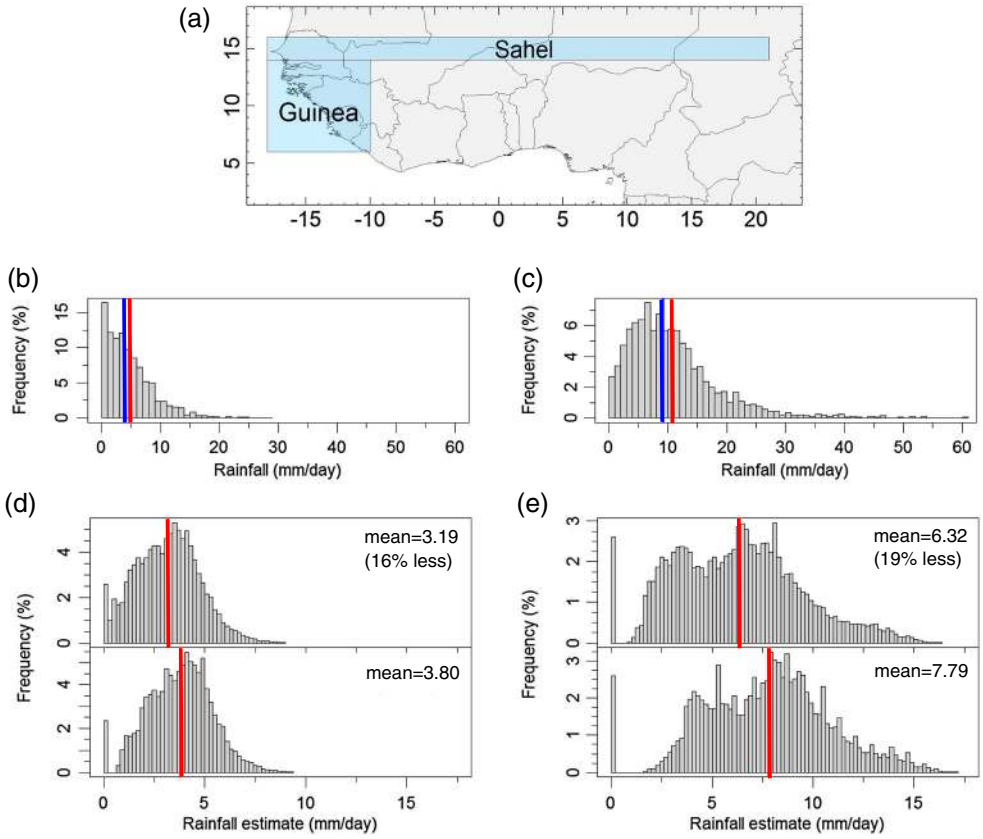


**Figure 6.** (a) Two August TAMSAT calibrations zones for West Africa; Sahel, and Guinea—chosen for their contrasting rainfall climates. Histograms of gauge observations used in the TAMSAT calibrations for the (b) Sahel zone and (c) Guinea zone. Histograms of all the August TAMSAT rainfall estimates (pixel resolution) from 1983 to 2012 over the (d) Sahel zone and (e) Guinea zone calculated when calibrated using median rainfall (top) and mean rainfall (bottom). Blue (red) vertical lines denotes median (mean) rainfall.

typically skewed toward low values, the median rainfall is chosen as it is insensitive to the occasional high rainfall event, while being more representative of typical, lower rainfall amounts. The latter has been demonstrated in studies such as *Dinku et al.* [2007], *Jobard et al.* [2011], and *Maidment et al.* [2013] and in Figure 3f. This approach, however, leads to an overall dry bias as median rainfall is almost always less than mean rainfall (e.g., Figure 6) and becomes more apparent when rainfall totals are integrated over large temporal and spatial scales (e.g., annual and Africa wide). While selecting the mean rainfall would yield estimates similar to those given by the other data sets, it would usually result in higher rainfall (as opposed to using the median rainfall) for any given amount of CCD and therefore overestimate the more frequent low rainfall amounts. For example, using monthly GPCC-FDR rainfall (August data from 1983 to 2010 across West Africa between 10°N and 20°N) as the reference, rainfall amounts of 5 mm $d^{-1}$ or less were overestimated by 0.54 mm $d^{-1}$ on average when CCD were calibrated using the mean rainfall, as opposed to an overestimate of just 0.06 mm $d^{-1}$ when using the median rainfall (not shown). The reduced skill this would have during low rainfall dekads is undesirable for drought monitoring, and therefore, the observed underestimation in total precipitation caused by using median rainfall is not corrected for.

The amount by which the TAMSAT algorithm underestimates rainfall varies according to the rainfall characteristics of different regions. This is demonstrated in Figure 6 where two West Africa regions are contrasted for August. The Sahel zone (Figure 6b) is characterized by a narrower distribution of rainfall amounts compared to the Guinea zone (Figure 6c). This implies that the amount by which the median rainfall (blue line in Figures 6b and 6c) is lower than the mean rainfall (red line in Figures 6b and 6c) will be greater over the Guinea zone than over the Sahel zone, resulting in a larger dry bias over the former. This is evident in Figure 4 when TARCAT is compared to the other data sets. Calibrating the CCD using the median rainfall results in an

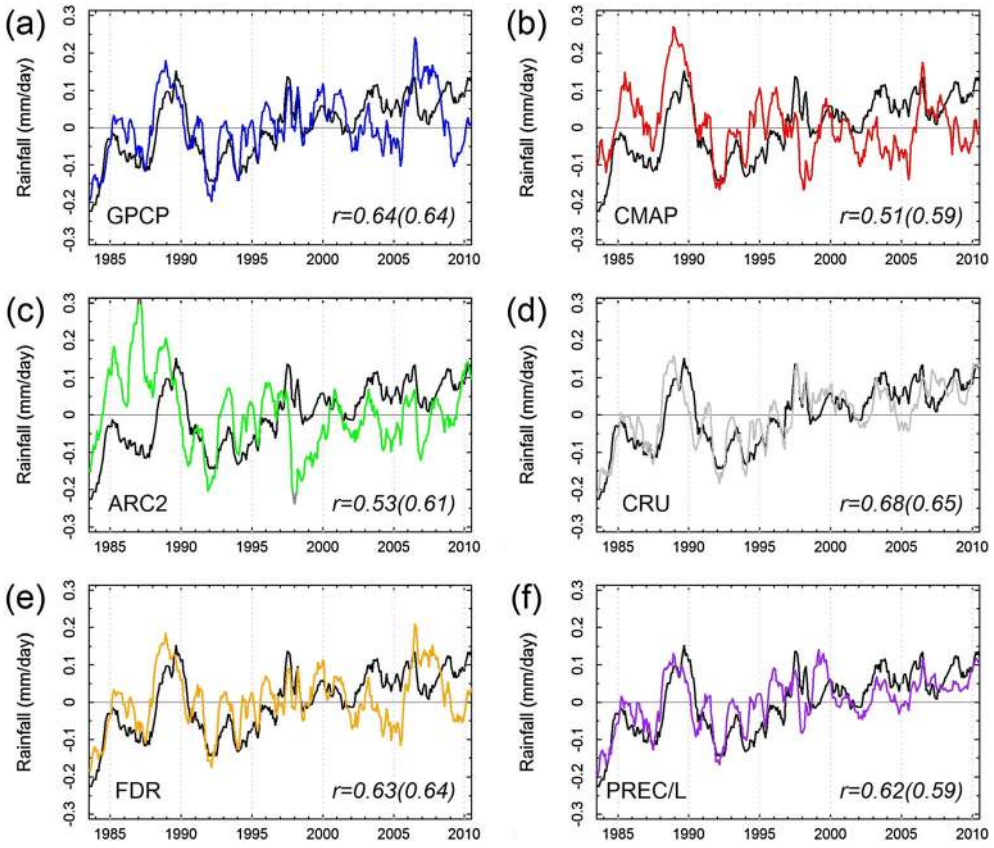


**Figure 7.** Twelve month running mean of deseasonalized Africa-wide area-average monthly rainfall for (a) GPCP, (b) CMAP, (c) ARC2, (d) CRU, (e) GPCC-FDR, and (f) PREC/L compared to TARCAT (black solid line). Shown are the correlations between the deseasonalized monthly rainfall. Values in parentheses denote the correlation where linear detrending to the time series has been applied.

underestimate of 16% and 19% over the Sahel and Guinea coastal zones respectively, as opposed to when CCD is calibrated using the mean rainfall instead (Figures 6d and 6e); this difference is similar in magnitude to the average difference between TARCAT and the other data sets considered.

The effect of nonconvective or warm rain (denoted here as rain from cloud tops warmer than what is considered cold cloud by the algorithm) which is known to occur over the Guinea zone [*Herman et al*., 1997; *Nicholson et al*., 2003b; *Schumacher and Houze*, 2003, 2006; *Sealy et al*., 2003; *Liu and Zipser*, 2009] and orographic enhancement over the Guinea Highlands results in the observed rainfall distribution of this region. Usually, the average contribution warm rain and or orographic enhancement provides is taken into account during the calibration stage (provided cold cloud is present during the 10 day period) by increasing the intercept coefficient ($a_0$). However, on inspection of gauge records and coincident CCD values over the Guinea zone (not shown), high rainfall events are not always associated with high CCD values. This indicates that warm rain and orographic enhancement cause or at least contribute to the high rainfall events and thus the relatively large underestimation by TARCAT over this region of West Africa. Because the accuracy of TARCAT is based on the premise that rainfall is closely associated with the occurrence of cold cloud tops of deep convective systems (see section 1), TARCAT is likely to be less skilful in locations where rainfall from shallow convective systems and warm rain processes are important, such as the Guinea Coast, northern Madagascar, and over the complex topography of the Ethiopia Highlands.

Another possible source of underestimation is that no gauge corrections have been applied to the gauge records used in the TAMSAT calibrations. These corrections attempt to correct for an undercatch of the actual rainfall due to both instrument and certain weather conditions [*Sevruk*, 1982; *Legates and Willmott*, 1990]. However, the magnitude of these corrections is likely to be relatively small in the Tropics because of high rainfall intensities, lower wind speeds, and no snowfall—conditions which are typically not associated with causing a significant undercatch

**Table 5.** Data Set Correlation Matrix of the Area-Average Monthly (Below Diagonal) and Annual (Above Diagonal) Rainfall Anomalies From 1983 to 2010[a]

| | TARCAT | GPCP | CMAP | ARC2 | CRU | FDR | PREC/L |
|---|---|---|---|---|---|---|---|
| TARCAT | - | **0.69** (**0.68**) | 0.41 (**0.71**) | 0.28 (**0.52**) | **0.85** (**0.77**) | **0.70** (**0.71**) | **0.80** (**0.72**) |
| GPCP | **0.64** (**0.64**) | - | **0.77** (**0.88**) | 0.42 (**0.50**) | **0.85** (**0.86**) | **0.98** (**0.98**) | **0.84** (**0.83**) |
| CMAP | **0.51** (**0.59**) | **0.85** (**0.87**) | - | **0.63** (**0.61**) | **0.54** (**0.76**) | **0.81** (**0.92**) | **0.65** (**0.85**) |
| ARC2 | **0.53** (**0.61**) | **0.68** (**0.70**) | **0.74** (**0.74**) | - | 0.37 (**0.55**) | 0.47 (**0.54**) | 0.42 (**0.58**) |
| CRU | **0.68** (**0.65**) | **0.84** (**0.84**) | **0.70** (**0.75**) | **0.60** (**0.64**) | - | **0.87** (**0.88**) | **0.91** (**0.87**) |
| FDR | **0.63** (**0.64**) | **0.99** (**0.98**) | **0.85** (**0.87**) | **0.68** (**0.70**) | **0.84** (**0.85**) | - | **0.88** (**0.88**) |
| PRECL | **0.62** (**0.59**) | **0.80** (**0.79**) | **0.73** (**0.77**) | **0.64** (**0.67**) | **0.80** (**0.79**) | **0.80** (**0.80**) | - |

[a]The monthly anomaly has been computed by subtracting the monthly climatological values from each month while the annual anomaly represents the deviation from the long-term average. Both climatologies were computed from 1983 to 2010. Values in parentheses denote the correlation where the time series has been detrended while values in bold indicate statistically significant correlations at the 99% level.

in rainfall measured by gauges. Since adjustments for possible rainfall undercatch are applied to GPCC-FDR [*Schneider et al*., 2014] but not to CRU or PREC/L and that all three products have similar annual and seasonal mean rainfall (see Table 4), suggests that accounting for rain gauge undercatch is not that important over Africa.

### 4.3. Interannual Variability

In the following we present the interannual variability of TARCAT and the six comparison precipitation data sets. The 12 month running average of deseasonalized Africa-wide area-average monthly rainfall is given in Figure 7 (data set correlation matrix of the monthly and annual rainfall anomalies is given in Table 5). It is evident that there are differences between the data sets, emphasizing the sensitivity of rainfall estimates (and inferred trends) to the methodology of generating the data set.

TARCAT closely follows the gauge-only data sets, particularly CRU, where both the short and long-term changes are tracked well. Correlations of 0.68 and 0.85 with CRU were found for the monthly and annual rainfall anomalies respectively. A wetting trend during the whole period is evident in both products (CRU: 22.9 mm decade$^{-1}$; TARCAT: 27.8 mm decade$^{-1}$), consistent with a gradual cooling of the 3rd percentile in the Meteosat TIR record in Figure 1d and Table 2. Even with this positive trend removed, respectable correlations of 0.65 (monthly) and 0.77 (annual) with CRU were found. Correlations of 0.63 and 0.70 were found with FDR for the monthly and annual totals respectively. This level of agreement suggests that TARCAT is sensitive to year-to-year and long-term changes in rainfall, despite the initial concerns that TIR calibration uncertainties may conceal such signals and the use of a climatological calibration may fail to accurately capture interannual fluctuations in rainfall. Since GPCP and CMAP incorporate gauge information (GPCC gauge analysis) in their final estimates, the correlations with the gauge-only data sets are higher than TARCAT. Despite the fact that it includes merging with contemporaneous gauge data, ARC2 has similar correlation coefficients to TARCAT with the gauge-only data sets at monthly scales but TARCAT correlation coefficients are greater at annual totals (e.g., the correlation with GPCC-FDR is 0.70 for TARCAT and 0.47 for ARC2).

While some of the disagreement between TARCAT and the other data sets is caused by limitations of the TAMSAT algorithm, there are also errors in the other data sets. For example, although it is to be expected that the gauge-only data sets agree well with each other, there appears to be less agreement between CRU, GPCC-FDR, and PREC/L during 2000–2010. The lower agreement coincides with a sharp drop off in gauge coverage and thus perhaps reflects sampling errors arising from fewer gauges in this period compared to earlier decades.

In summary, these analyses demonstrate that despite some limitations of the TAMSAT algorithm, TARCAT skillfully represents interannual and decadal variability.

## 5. Discussion

Improving our understanding of the present and historical rainfall climate across Africa is required as there is large uncertainty in how rainfall in this part of the world is responding to a warming climate. Furthermore, real-time monitoring of the rainy season is important in many sectors, but detection of above or below average rainfall is only possible through reliable long-term climatologies.

The scarcity of records from the existing gauge network means that the current rainfall climatology across Africa is poorly understood compared to other regions such as Europe and North America. Satellite-based rainfall data sets exist, some of which have shown to perform well in parts of Africa, but many of these only cover short time spans and thus cannot yet be used to infer long-term variability. Those covering longer time spans merge rain gauge data contemporaneously. Arguably, such an approach makes maximal use of both satellite and gauge data, and indeed, these data sets have proved invaluable tools for the operational monitoring of rainfall, both for flood and drought applications [e.g., *Herman et al*., 1997; *Verdin et al*., 2005; *Novella and Thiaw*, 2013]. In Africa, however, the temporal inconsistency of the gauge record means that products that merge contemporaneous data may not robustly represent rainfall trends over long periods. The lack of independent gauge data means that it is difficult to quantify the effect of this artifact in Africa. However, the systematic bias introduced by changing gauge coverage has been demonstrated, for example, in *Balan Sarojini et al*. [2012] and *Wan et al*. [2013].

By using a historical calibration rather than merging contemporaneous data, the TARCAT data set provides a complementary approach to the existing products. TARCAT loses some skill by not merging contemporaneous gauge data. It cannot, for example, represent individual extreme rainy events and thus underestimates variability which data sets that merge contemporaneous gauge data, such as GPCP, CMAP, and ARC2, may represent better where gauge coverage is sufficient. Countering this, the long-term trends inferred from TARCAT are not biased by temporally inconsistent gauge records, and the rainfall monitoring product, TAMSAT, is not corrupted by individual inaccurate gauge readings.

Given the differences between existing gauge and satellite-based rainfall data sets, such as demonstrated in this study, objective intercomparisons of all available data sets is required to quantitatively evaluate rainfall patterns and trends over Africa. Only then, can steps be made to further our understanding of the processes controlling rainfall variability and improve our knowledge of the rainfall climate.

## 6. Conclusions

Since Meteosat TIR data have been available since the early 1980s, it has been possible to generate a time series of rainfall estimates for the last 30 years using a consistent algorithm for all of Africa known as TARCAT —a more complete and consistent time series of TAMSAT rainfall estimates than has previously been possible. An evaluation of the Meteosat TIR archive has demonstrated that few significant time-dependent biases exist as a result of multiple satellites operating during the Meteosat Earth observation program suggesting the instruments' calibration are stable over time. An intercomparison of TARCAT and six widely used satellite and gauge long-term rainfall data sets demonstrated that TARCAT does well in replicating the mean spatial and seasonal rainfall patterns and following the interannual variability over 1983 to 2010. However, optimizing TAMSAT's calibration approach for drought leads to estimates having an Africa-wide average dry bias of ~20% relative to other widely used data sets.

TARCAT differs from existing long-term data sets because the data inputs and calibration do not change from year to year. The omission of contemporaneous gauge information is compensated for by the derivation of regional and monthly calibration parameters that ensure the estimates are tuned to the local rainfall climate. TARCAT is therefore a useful complement to existing products. As TARCAT only requires Meteosat TIR imagery and is updated in near real-time (every 10 days), it also serves as a valuable monitoring product that has a climatology based on over 30 years of observations [e.g., *Boyd et al*., 2013, Figure 1; *Kucera et al*., 2013, Figure 7]. This is especially the case over gauge-sparse regions and in places where political instability may jeopardize timely access to gauge measurements. The provision of the TARCAT data at 10 day totals and 0.0375° spatial resolution, which can be aggregated to resolutions that meet users' requirements make TARCAT suitable for regional/district level and drought/agricultural applications, sectors where reliable and timely rainfall data are especially needed.

The current version of the TARCAT data set represents the first attempt at generating a long-term rainfall data set using the TAMSAT algorithm. As more historic gauge data becomes available, further improvements in the calibration and independent validations are planned. Identifying changes in the rainfall climate will also help diagnose whether time-varying amendments to the calibration are required. The current calibration approach could also be adapted for other purposes (e.g., hydrological monitoring) where rainfall information is required but is impeded by difficulty in accessing historical and/or real-time gauge information.

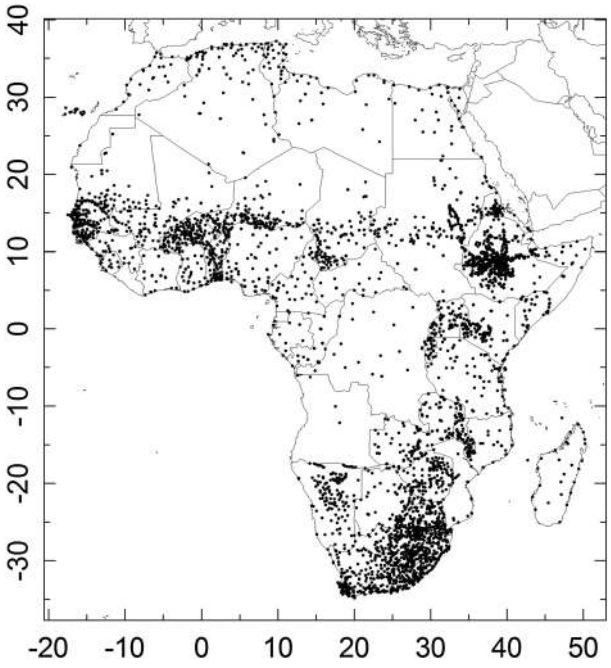


**Figure A1.** The distribution of the gauge network (approximately 4300 stations) used to derive the TAMSAT calibrations. Each gauge is represented by a dot.

## Appendix A: Derivation of the TAMSAT Calibration Parameters

The derivation of the regional and monthly calibration parameters has been performed in three stages as follows: (1) identification of calibration zones, (2) selection of the optimum temperature threshold $T_t$ for each zone, and (3) obtaining the regression parameters slope ($a_0$) and offset ($a_1$) for each zone. For this purpose, coincident cold cloud duration (CCD) pixels (at temperature thresholds of 213 K, 223 K, 233 K, and 243 K) are extracted for each rain gauge location (see Figure A1) where a 10 day rainfall total record is available.

### A1. Stage 1: Identification of Calibration Zones

The TAMSAT estimation method is based on calibration zones that vary spatially and seasonally to reflect changes in the rainfall climate. The variation in rainfall climate is largely determined by the passage of the ITCZ, modulated locally by features such as topography and proximity to lakes and the ocean. Such variations imply changes in the average storm characteristics and hence CCD-rainfall relationships [*Dugdale et al*., 1991; *Todd et al*., 1995, 1999; *Dybkjær*, 2003; *Chadwick et al*., 2010]. Temporal variations are dealt with by producing calibrations for each calendar month. It is assumed that the rainfall climate across each zone is climatologically homogeneous; hence, the calibration parameters $T_t$, $a_1$, and $a_0$ remain constant across each zone.

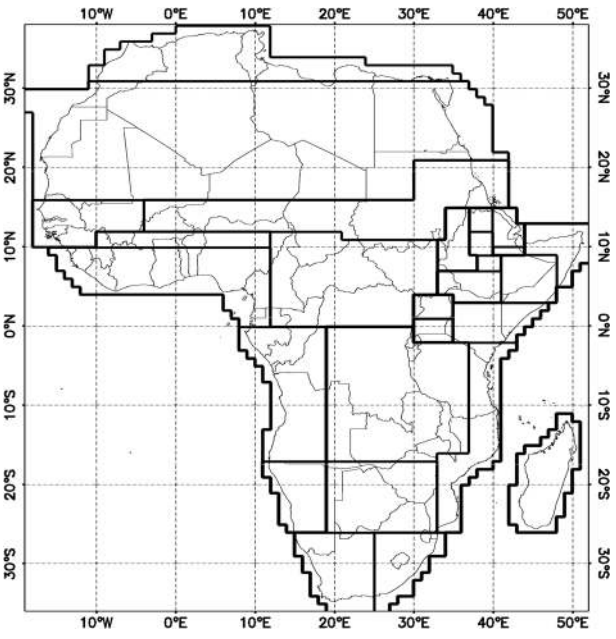


**Figure A2.** The TAMSAT calibration zones for May. For this month, Africa including Madagascar, has been split into 27 zones. Zone boundaries and the number of zones vary for each calendar month.

Zones are empirically determined using gauge observations. The frequency bias between all gauge-CCD pairs (at each of the four temperature thresholds) is calculated based on rainfall and CCD occurrence at thresholds of 0 mm and 0 h respectively. Inspection of the spatial variation of these point-based bias scores provides the basis of the zone boundaries. Supporting information such as topography and knowledge of the local climate allows these boundaries to be tuned accordingly, particularly where gauge observations are sparse or nonexistent. Due to the constraints posed by a sparse gauge network, defining the zones is based on a compromise between making the zones small enough to represent the local climate while being large enough to contain sufficient gauges to generate a robust calibration. An example of the calibration zones for May is given in Figure A2.

**Table A1.** Contingency Table for Determining $T_t$

| | CCD = 0 | CCD > 0 |
|---|---|---|
| Gauge = 0 | $n_{11}$ | $n_{12}$ |
| Gauge > 0 | $n_{21}$ | $n_{22}$ |

### A2. Stage 2: Selection of the Optimum Temperature Threshold for Each Zone

The optimum temperature threshold $T_t$ is defined as the cloud top temperature that best distinguishes between rain and no rain. For selecting the appropriate $T_t$, all gauge-CCD pairs within each zone are sorted into contingency tables where the $T_t$ corresponding to the highest level of agreement between rainfall and CCD occurrence is chosen according to the criteria given in Table A1 and equations (A1) and (A2). The occurrence threshold is set at zero for both rainfall (mm) and CCD (hours). All gauge-CCD pairs are split into one of four possible groups with the counts for each group recorded. Each group ($n$11:$n$22) is defined as follows.

1. $n_{11}$ is the number of occasions where both zero rainfall and CCD is observed.
2. $n_{12}$ is the number of occasions where zero rainfall is recorded but CCD is detected.
3. $n_{21}$ is the number of occasions where rainfall is recorded but no CCD is detected.
4. $n_{22}$ is the number of occasions where both rainfall and CCD are greater than zero.

Given the above criteria, $n_{11}$ and $n_{22}$ correspond to agreement between the gauge and CCD while $n_{12}$ and $n_{21}$ represent disagreement. Therefore, for the selection of $T_t$, the occasions of agreement need to be significantly higher than occasions of disagreement. Furthermore, since $n_{12}$ counts represent false alarms (i.e., algorithm gives nonzero CCD when no rainfall was observed, resulting in overestimation of rainfall) and $n_{21}$ counts represent misses (i.e., algorithm gave zero CCD hours when rainfall was observed, resulting in underestimation of rainfall), ideally $n_{12}$ and $n_{21}$ should be roughly equal in magnitude so that these biases in rainfall occurrence compensate. Thus, the conditions for selecting $T_t$ are

$$n_{11} + n_{22} \gg n_{12} + n_{21} \tag{A1}$$

$$n_{12} \cong n_{21} \tag{A2}$$

This procedure is carried out at each of the four temperature thresholds considered and repeated for each zone for all calendar months.

### A3. Stage 3: Obtaining the Regression Parameters for Each Zone

After selection of $T_t$, a regression is carried out on all gauge-CCD pairs for CCD values at the chosen $T_t$. Regression is only carried out for CCD values greater than zero. A minimum of 100 gauge-CCD pairs have been suggested for generating a reliable calibration [*Dugdale et al.*, 1991; *Milford et al.*, 1996]. The CCD data are binned to reduce the large amount of scatter between gauge-CCD pairs before a linear model is fitted to the data to obtain the linear regression parameters $a_0$ and $a_1$. The median rainfall for given CCD bins is chosen to regress against the midpoint for each CCD bin, weighted by the number of gauge-CCD pairs in each bin. This step is repeated for each zone for all calendar months. Other models such as quadratic and logarithmic and the use of multiple regression have previously been tested, but did not yield significantly better results to warrant a change to the regression approach [*Dugdale et al.*, 1991; *Milford et al.*, 1996].

The zone definition approach results in spatial discontinuities between zones in the rainfall estimates. Artificial smoothing between the zones boundaries (applied over distances of 1 or 0.5°, depending on the size of the zone) of the calibration parameters is applied to help reduce this, although discontinuities inevitably persist. Despite the visual problems, the block approach attempts to establish the optimal CCD-rainfall relationship across many years for a given location, given the available gauge data. In reality, variations in the CCD-rainfall relationship may change gradually as a function of space, but representing this Africa wide in the calibration is limited by a lack of gauges. However, the block method used makes optimal use of existing gauges, especially where few exist. When interpreting spatial variability from TAMSAT data, the existence of these discontinuities should be accounted for. Nevertheless, the rainfall estimates, devised using this calibration approach, have greater skill than if a single homogeneous calibration is used, even though the data would undoubtedly have a more spatially homogeneous appearance.

The reliability of the calibration parameters is dependent upon the availability of the gauge records which presents a problem in areas such as the Congo Basin and Angola. Here calibration parameters are based on the available data and neighboring calibration zones.

## Appendix B: Formulae for Quantifying Errors

Quantification of the differences between the perturbed and unperturbed rainfall estimates in sections 3.3 and 3.4 were based on at least one of the following error statistics; mean error (ME), mean absolute error (MAE), mean absolute percentage error (MAPE), root-mean-square error (RMSE), and percentage root-mean-square error (PRMSE). Error analysis was performed on a pixel basis for each rainfall dekad according to the formulae given below:

$$\mathrm{ME} = \frac{1}{N}\sum_{i=1}^{N}(P_i - O_i) \tag{B1}$$

$$\mathrm{MAE} = \frac{1}{N}\sum_{i=1}^{N}(|P_i - O_i|) \tag{B2}$$

$$\mathrm{MAPE} = \frac{100}{N}\sum_{i=1}^{N}\left(\frac{|P_i - O_i|}{O_i}\right) \tag{B3}$$

$$\mathrm{RMSE} = \sqrt{\frac{\sum_{i=1}^{N}(P_i - O_i)^2}{N}} \tag{B4}$$

$$\mathrm{PRMSE} = 100\overline{O}\sqrt{\frac{\sum_{i=1}^{N}(P_i - O_i)^2}{N}} \tag{B5}$$

where $P_i$ and $O_i$ represent respectively the perturbed rainfall estimate and operational rainfall estimate for pixel $i$ and $N$ is the total number of pixels in each rainfall field. Collocated zero rainfall pixels from the perturbed rainfall estimate and operational rainfall estimate were removed to restrict the study to rainy areas only over the African continent.

## Appendix C: Recovery of Missing Rainfall Dekads

### C1. Recovery Scheme 1: Extending the Temporal Interpolation Across Missing Slots

The TAMSAT method is able to cope with missing imagery by temporally interpolating between missing slots as described in section 3.3. The standard TAMSAT approach can allow up to 3 h of consecutive missing TIR slots, but we have increased the allowed gap to 6 h. Interpolating over such gaps will naturally lead to sampling errors, particularly if missing slots occur when the cloud top temperature is close to the cold cloud temperature threshold and/or if there is a rapid change in the cloud top temperature. *Dugdale et al*. [1991] demonstrated that accounting for a gap of 3 h by temporal interpolation gave the smallest error—as opposed to applying no correction or using observed cold cloud as a fraction of the daily total number of existing slots. To quantify the expected error when interpolating over 6 h, gaps were artificially introduced into the TIR archive for a period when all slots exist. The gaps introduced were centered on each hour over all 10 days in each dekad resulting in an ensemble of 240 estimates for the dekad. Each ensemble estimate was compared to the operational rainfall estimate, which used all available slots. Gaps of 3 and 9 h were also computed although the latter is not implemented into the TARCAT data set.

Table C1 provides the ensemble average for the mean absolute error (MAE) and root-mean-square error (RMSE) for each of the gap sizes considered for the three dekads in August 2008. At a resolution of 0.5°, an average RMSE of 0.04 mm $d^{-1}$ (0.83%) and 0.13 mm $d^{-1}$ (2.63%) were found for 3 and 6 h gaps respectively, although the sign of the mean error follows a diurnal cycle (Figure C1) explained by the daily cycle in convection and resulting cold cloud development which is dependent upon meteorological regime. Missing slots around

**Table C1.** Average Error Statistics When Gaps of 3, 6, and 9 h are Introduced Into the Satellite Archive[a]

| | | MAE | | RMSE | |
|---|---|---|---|---|---|
| Gap Introduced (h) | Spatial Resolution (°) | (mm/d) | (%) | (mm/d) | (%) |
| 3 | 0.0375 | 0.02 | 0.60 | 0.07 | 1.57 |
| 6 | 0.0375 | 0.06 | 1.79 | 0.18 | 3.90 |
| 9 | 0.0375 | 0.12 | 3.31 | 0.30 | 6.60 |
| 3 | 0.5 | 0.02 | 0.36 | 0.04 | 0.83 |
| 6 | 0.5 | 0.06 | 1.27 | 0.13 | 2.63 |
| 9 | 0.5 | 0.11 | 2.52 | 0.25 | 4.80 |

[a]Errors calculated based on all rainfall dekads and possible substitutions (see section 3.4 for details) at satellite pixel resolution (0.0375°) and a coarser resolution (0.5°). 720 dekads were used to compute each statistic. See Appendix B for error calculation details.

late morning tends to result in the largest overestimate in rainfall while the largest underestimate occurs during late afternoon/early evening. For other times, no particular sign of mean error is favored. Gaps of up to 6 h were found to occur randomly, irrespective of time of day suggesting no systematic bias results from this recovery scheme. To illustrate an example of this recovery scheme, Figure C2 gives the rainfall estimate for the 2nd dekad in August 2008 along with an example of the error when a gap of 6 h is removed (Figure C2b). This example reveals that at pixel resolution, differences greater than 2 mm $d^{-1}$ (~40%) exist; however, on average across all simulations with a gap of 6 h, 95% of rainy pixels are within 0.42 mm $d^{-1}$. There is, however, a tendency for errors of opposite sign to exist side by side such that spatial averaging minimizes these errors considerably (Figures C2b and C2c). Larger errors can be expected when few storm events or the existence of more than one gap exists in a dekad. Six hours was chosen as an increase to the maximum time to interpolate across as it allowed a further 99 dekads (~10%) to be recovered while the errors remain considerably less than the error in TAMSAT rainfall estimates reported in validation studies [*Laurent et al.*, 1998; *Dinku et al.*, 2007; *Chadwick et al.*, 2010; *Jobard et al.*, 2011; *Maidment et al.*, 2013]. These studies reported RMSE values in the range of 36% to 48% at 0.5° resolution; representative of the error arising from the indirect relationship between cloud top temperature and surface rainfall. Extending to 9 h was not implemented based on physical grounds as the likelihood of missing entire storms increases, evidence perhaps in a doubling of the error magnitude from 6 to 9 h, despite being only a 50% increment in time.

### C2. Recovery Scheme 2: Replacing the Missing Daily CCDs With the Dekad Mean

No daily cold cloud duration (CCD) fields have been calculated for gaps exceeding 6 h. For TARCAT, we have recovered a further 80 dekads (~8%) containing up to 2 days of missing CCD information by substituting the missing days with the mean from the remaining days in the respective dekad in the assumption that rainfall of the missing days is similar to that of the dekad. Such an approach has been used previously for TAMSAT estimates [*Dugdale et al.*, 1991] and offers a computationally easy approach that would otherwise result in no dekad estimate or would require supporting information such as gauges to supplement the

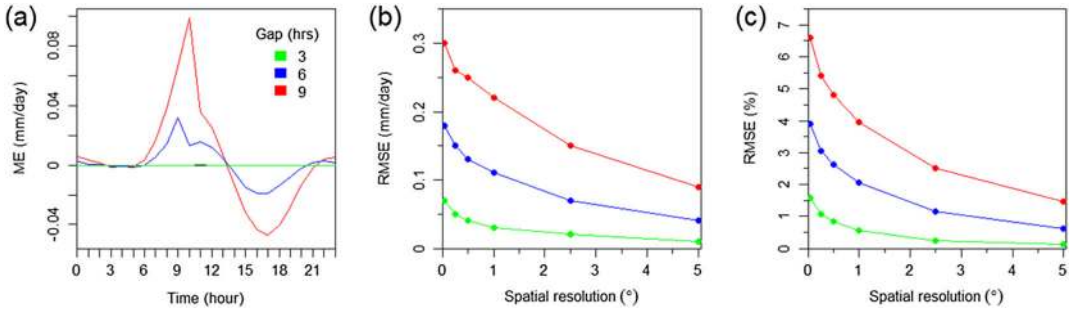


**Figure C1.** (a) The average ME across all simulations in the three dekads in August 2008 ($n = 760$) as a function of time of day when gaps of 3, 6, and 9 h are introduced into the satellite archive. The average RMSE as a function of spatial resolution expressed as (b) rainfall amount and (c) percentage.

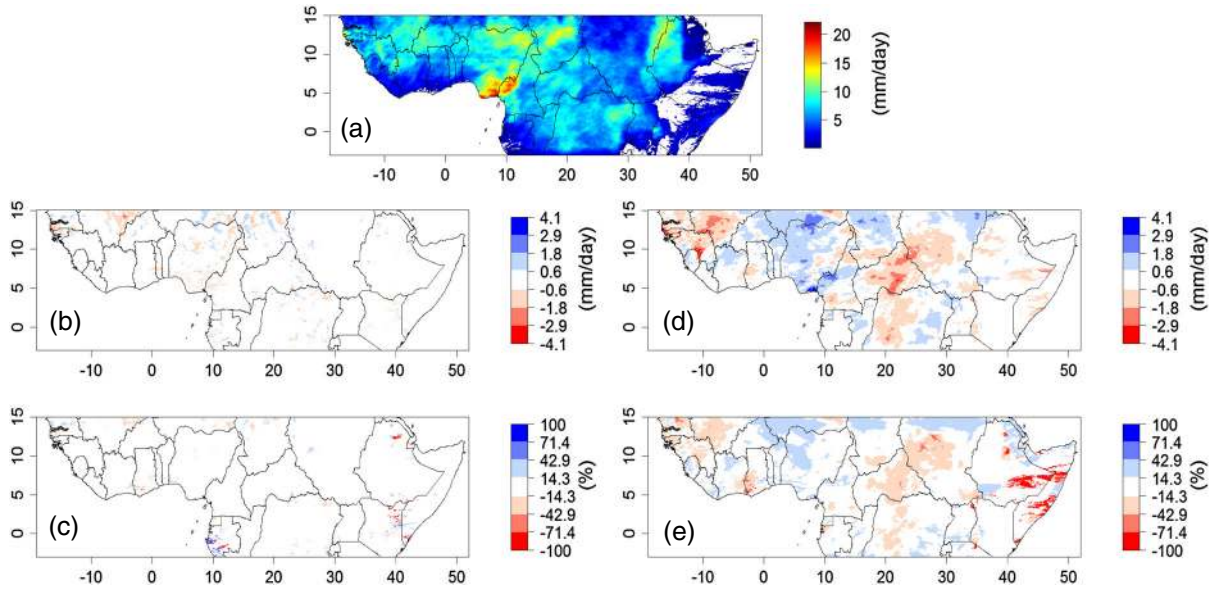


**Figure C2.** (a) The rainfall estimate for the 2nd dekad in August 2008, (b) the error between the original estimate (using all TIR slots, Figure C2a) and the estimate obtained when a 6 h gap is introduced into the satellite archive on the 4th day of the dekad centred at 18:00 h and (c) the corresponding percentage error, (d) the error between the original estimate (Figure C2a), and the estimate obtained when the 3rd and 9th days of CCD fields in the dekad are removed and replaced with the mean of the existing daily CCD fields in the dekad and (e) the corresponding percentage error.

missing days—which in itself would be a challenge. Estimates of the expected error were computed when up to three daily CCD fields were artificially removed (using a random sample of combinations ($n = 1000$) of missing days within a dekad for each number of days missing) from 36 dekads in 2000, 2002, and 2009 where all daily CCD fields exist.

Table C2 summarizes the ensemble of errors over all substitutions considered for 1, 2, and 3 days of CCD fields removed. An average RMSE of 0.42 mm $d^{-1}$ (11.4%) and 0.64 mm $d^{-1}$ (17.3%) are expected for 1 and 2 days missing respectively at 0.5° resolution. For 2 days missing at pixel resolution, 95% of rainy pixels are estimated within 1.32 mm $d^{-1}$, although spatial averaging reduces the errors (Figure C3). Of the years considered, there is no evidence to suggest that the errors vary significantly on an intraseasonal or interannual basis (not shown). This recovery scheme, illustrated in Figures C2d and C2e when two random days of CCD are removed, demonstrates that errors of opposite sign exist, although larger in spatial extent than Recovery Scheme 1. This occurs when the removed CCD field coincides with either a rainfall event or dry spell, which is not well represented by the mean of the remaining days resulting in an underestimate or overestimate respectively. Where many storms have passed, the relative error is typically small. However, large errors may

**Table C2.** Average Error Statistics When 1, 2, and 3 Days of Daily CCD Fields Were Removed From Complete Rainfall Dekads[a]

| | | MAE | | RMSE | |
|---|---|---|---|---|---|
| No. of Days Missing | Spatial Resolution (°) | (mm/d) | (%) | (mm/d) | (%) |
| 1 | 0.0375 | 0.26 | 11.11 | 0.41 | 13.64 |
| 2 | 0.0375 | 0.40 | 19.45 | 0.62 | 20.63 |
| 3 | 0.0375 | 0.54 | 27.20 | 0.81 | 27.15 |
| 1 | 0.5 | 0.29 | 9.51 | 0.42 | 11.44 |
| 2 | 0.5 | 0.46 | 15.84 | 0.64 | 17.30 |
| 3 | 0.5 | 0.60 | 21.59 | 0.83 | 22.86 |

[a]Error statistics calculated for all rainfall dekads and possible substitutions (see section 3.4 for details) from rainfall dekads in 2000, 2002, and 2009 at satellite pixel resolution (0.0375°) and a coarser resolution (0.5°). A random sample ($n = 1000$) was used to estimate the error for each number of days missing; hence, for 1 (2) day missing, 1096 (5027) substitutions were possible across the years sampled. See Appendix B for error calculation details.

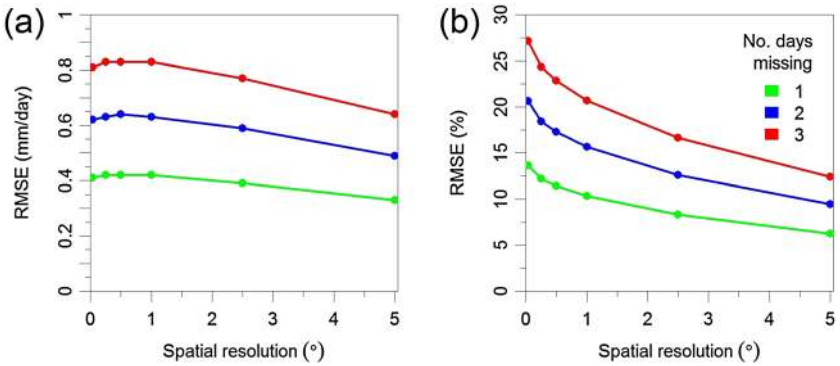


**Figure C3.** The average RMSE as a function of spatial resolution expressed as (a) rainfall amount and (b) percentage when 1, 2, and 3 days of CCD fields were removed from all dekads across 2000, 2002, and 2009.

result if there are few or only a single rainfall event within a dekad that happens to correspond with the missing daily CCD field(s). While the errors for this method are greater than those from the first recovery scheme, they are still less than half of the typical range in errors associated with TAMSAT rainfall estimates [*Laurent et al*., 1998; *Dinku et al*., 2007; *Chadwick et al*., 2010; *Jobard et al*., 2011; *Maidment et al*., 2013]. The recovery scheme was not extended to 3 days for an obvious increase in error and that only less than 1% of dekads would be recovered.

**Acknowledgments**

We dedicate this paper to the legacy in African rainfall monitoring and its societal importance left by our coauthor and friend, David Grimes, who sadly passed away on 22 December 2011 and whom a great many people sorely miss. The TARCAT data set, updated at the end of every dekad, is available from the TAMSAT website (http://www.met.reading.ac.uk/~tamsat/data). Meteosat TIR data can be ordered directly from EUMETSAT. TAMSAT does not have sharing rights for the rain gauge data used in calibration of the data set; therefore, readers are advised to contact African Meteorological and Hydrological Centers for access to this data. This investigation was supported with funding from a NERC (Natural Environment Research Council) PhD Studentship for quality controlling the Meteosat TIR data archive provided by EUMETSAT. Funding was also provided by NCEO (National Centre for Earth Observation). The authors would like to thank the European Commission's MARS (Monitoring of Agricultural Resources) Unit at the Joint Research Centre (JRC) in Ispra, Italy, for their valuable contribution to the development of the TARCAT data set.

## References

Adler, R. F., G. J. Huffman, and P. R. Keehn (1994), Global tropical rain estimates from microwave-adjusted geosynchronous IR data, *Remote Sens. Rev.*, *11*(1–4), 125–152, doi:10.1080/02757259409532262.

Adler, R. F., et al. (2003), The Version-2 Global Precipitation Climatology Project (GPCP) monthly precipitation analysis (1979–Present), *J. Hydrometeorol.*, *4*(6), 1147–1167, doi:10.1175/1525-7541(2003)004<1147:TVGPCP>2.0.CO;2.

Allan, R. P., A. Slingo, S. F. Milton, and M. E. Brooks (2007), Evaluation of the Met Office global forecast model using Geostationary Earth Radiation Budget (GERB) data, *Q. J. R. Meteorol. Soc.*, *133*(629), 1993–2010, doi:10.1002/qj.166.

Arkin, P. A., and B. N. Meisner (1987), The relationship between large-scale convective rainfall and cold cloud over the Western Hemisphere during 1982-84, *Mon. Weather Rev.*, *115*(1), 51–74, doi:10.1175/1520-0493(1987)115<0051:TRBLSC>2.0.CO;2.

Balan Sarojini, B., P. A. Stott, E. Black, and D. Polson (2012), Fingerprints of changes in annual and seasonal precipitation from CMIP5 models over land and ocean, *Geophys. Res. Lett.*, *39*, L21706, doi:10.1029/2012GL053373.

Becker, A., P. Finger, A. Meyer-Christoffer, B. Rudolf, K. Schamm, U. Schneider, and M. Ziese (2013), A description of the global land-surface precipitation data products of the Global Precipitation Climatology Centre with sample applications including centennial (trend) analysis from 1901–present, *Earth Syst. Sci. Data*, *5*, 71–99, doi:10.5676/DWD.

Benson, C., and E. J. Clay (1998), The impact of drought on sub-Saharan African economies: A preliminary examination, *World Bank Publ.*, *1*, WTP401.

Bergès, J., I. Jobard, F. Chopin, and R. Roca (2010), EPSAT-SG: A satellite method for precipitation estimation; its concepts and implementation for the AMMA experiment, *Ann. Geophys.*, *28*, 289–308.

Boyd, E., R. Cornforth, and P. Lamb (2013), Building resilience to face recurring environmental crisis in African Sahel, *Nat. Clim. Chang.*, *3*, 631–637, doi:10.1038/NCLIMATE1856.

Chadwick, R. S., D. I. F. Grimes, R. W. Saunders, P. N. Francis, and T. A. Blackmore (2010), The TAMORA algorithm: Satellite rainfall estimates over West Africa using multi-spectral SEVIRI data, *Adv. Geosci*, *25*, 3–9.

Chen, M., and P. Xie (2002), Global land precipitation: A 50-yr monthly analysis based on gauge observations, *J. Hydrometeorol.*, *3*, 249–266.

Christensen, J. H., et al. (2007), Regional climate projections, in *Climate Change 2007: The Physical Science Basis. Contribution of Working Group I to the Fourth Assessment Report of the Intergovernmental Panel on Climate Change*, edited by S. Solomon et al., Cambridge Univ. Press, Cambridge, U. K., and New York.

Cooper, P. J. M., J. Dimes, K. P. C. Rao, B. Shapiro, B. Shiferaw, and S. Twomlow (2008), Coping better with current climatic variability in the rain-fed farming systems of sub-Saharan Africa: An essential first step in adapting to future climate change?, *Agric. Ecosyst. Environ.*, *126*(1–2), 24–35, doi:10.1016/j.agee.2008.01.007.

Dinku, T., P. Ceccato, E. Grover-Kopec, M. Lemma, S. J. Connor, and C. F. Ropelewski (2007), Validation of satellite rainfall products over East Africa's complex topography, *Int. J. Remote Sens.*, *28*(7), 1503–1526, doi:10.1080/01431160600954688.

Dinku, T., S. Chidzambwa, P. Ceccato, S. J. Connor, and C. F. Ropelewski (2008), Validation of high-resolution satellite rainfall products over complex terrain, *Int. J. Remote Sens.*, *29*(14), 4097–4110, doi:10.1080/01431160701772526.

Diro, G. T., D. I. F. Grimes, E. Black, A. O'Neill, and E. Pardo-Iguzquiza (2009), Evaluation of reanalysis rainfall estimates over Ethiopia, *Int. J. Climatol.*, *29*(1), 67–78, doi:10.1002/joc.1699.

Doelling, D. R., L. Nguyen, and P. Minnis (2004), On the use of deep convective clouds to calibrate AVHRR data, in *Earth Observing Systems IX*, edited by W. L. Barnes and J. J. Butler, *Proc. SPIE*, *5542*, 281–289, doi:10.1117/12.560047.

Dugdale, G., V. D. McDougall, and J. R. Milford (1991), Rainfall estimates in the Sahel from cold cloud statistics: Accuracy and limitations of operational systems (Proceedings of the Niamey Workshop, February 1991), *Soil Water Balanc. Sudano-Sahelian Zo.*, (IAHS 199), 65–74.

Dybkjær, G. (2003), A simple self-calibrating cold cloud duration technique applied in West Africa and Bangladesh, *Geogr. Tidsskr.*, *103*(1), 83–98.

Fauchereau, N., S. Trzaska, M. Rouault, and Y. Richard (2003), Rainfall variability and changes in Southern Africa during the 20th century in the global warming context, *Nat. Hazards*, *29*(2), 139–154, doi:10.1023/A:1023630924100.

Flato, G., et al. (2013), Evaluation of climate models, in *Climate Change 2013: The Physical Science Basis. Contribution of Working Group I to the Fifth Assessment Report of the Intergovernmental Panel on Climate Change*, edited by T. F. Stocker et al., Cambridge Univ. Press, Cambridge, U. K., and New York.

Flitcroft, I. D., J. R. Milford, and G. Dugdale (1989), Relating point to area average rainfall in semiarid West Africa and the implications for rainfall estimates derived from satellite data, *J. Appl. Meteorol.*, *28*(4), 252–266, doi:10.1175/1520-0450(1989)028<0252:RPTAAR>2.0.CO;2.

Funk, C., and J. Verdin (2003), Comparing satellite rainfall estimates and reanalysis precipitation fields with station data for western Kenya, in *JRC-FAO International Workshop on Crop and Rangeland Monitoring in Eastern Africa for Early Warning and Food Security in Africa*, *Nairobi*, *January 28–30*, *2003*. *European Commission and FAO*, pp. 89–96.

Goldberg, M., et al. (2011), The Global Space-Based Inter-Calibration System, *Bull. Am. Meteorol. Soc.*, *92*(4), 467–475, doi:10.1175/2010BAMS2967.1.

Govaerts, Y., A. Arriaga, and J. Schmetz (2001), Operational vicarious calibration of the MSG/SEVIRI solar channels, *Adv. Sp. Res.*, *28*(1), 21–30.

Grimes, D. I. F., E. Pardo-Igúzquiza, and R. Bonifacio (1999), Optimal areal rainfall estimation using raingauges and satellite data, *J. Hydrol.*, *222*(1–4), 93–108, doi:10.1016/S0022-1694(99)00092-X.

Grimes, D. I. F., E. Coppola, M. Verdecchia, and G. Visconti (2003), A neural network approach to real-time rainfall estimation for Africa using satellite data, *J. Hydrometeorol.*, *4*(6), 1119–1133, doi:10.1175/1525-7541(2003)004<1119:ANNATR>2.0.CO;2.

Harris, I., P. D. Jones, T. J. Osborn, and D. H. Lister (2014), Updated high-resolution grids of monthly climatic observations - the CRU TS3.10 Dataset, *Int. J. Climatol.*, *34*(3), 623–642, doi:10.1002/joc.3711.

Heinemann, T., and V. Gärtner (2012), EUMETSAT'S role in the provision of precipitation related satellite data, in *International Precipitation Working Group* (*IPWG*) *Meeting*, São José dos Campos, Brazil.

Herman, A., V. B. Kumar, P. A. Arkin, and J. V. Kousky (1997), Objectively determined 10-day African rainfall estimates created for famine early warning systems, *Int. J. Remote Sens.*, *18*(10), 2147–2159, doi:10.1080/014311697217800.

Hewison, T. J. (2013), An evaluation of the uncertainty of the GSICS SEVIRI-IASI intercalibration products, *IEEE Trans. Geosci. Remote Sens.*, *51*(3), 1171–1181, doi:10.1109/TGRS.2012.2236330.

Hewison, T. J., and J. Muller (2013), Ice contamination of Meteosat/SEVIRI implied by intercalibration against Metop/IASI, *IEEE Trans. Geosci. Remote Sens.*, *51*(3), 1182–1186, doi:10.1109/TGRS.2012.2236335.

Hewison, T. J., X. Wu, F. Yu, Y. Tahara, X. Hu, D. Kim, and M. Koenig (2013), GSICS inter-calibration of infrared channels of geostationary imagers using Metop/IASI, *IEEE Trans. Geosci. Remote Sensing*, *51*(3), 1160–1170, doi:10.1109/TGRS.2013.2238544.

Hoerling, M., J. Hurrell, J. Eischeid, and A. Phillips (2006), Detection and attribution of twentieth-century Northern and Southern African rainfall change, *J. Clim.*, *19*(16), 3989–4008, doi:10.1175/JCLI3842.1.

Hsu, K.-L., and S. Sorooshian (2008), Satellite-based precipitation measurement using PERSIANN system, in *Hydrological Modelling and the Water Cycle*, vol. 63, pp. 27–48, Springer, Berlin, Heidelberg.

Huffman, G. J., R. F. Adler, P. Arkin, A. Chang, R. Ferraro, A. Gruber, J. Janowiak, A. McNab, B. Rudolf, and U. Schneider (1997), The Global Precipitation Climatology Project (GPCP) combined precipitation dataset, *Bull. Am. Meteorol. Soc.*, *78*(1), 5–20, doi:10.1175/1520-0477(1997)078<0005:TGPCPG>2.0.CO;2.

Huffman, G. J., R. F. Adler, M. M. Morrissey, D. T. Bolvin, S. Curtis, R. Joyce, B. McGavock, and J. Susskind (2001), Global precipitation at one-degree daily resolution from multisatellite observations, *J. Hydrometeorol.*, *2*(1), 36–50, doi:10.1175/1525-7541(2001)002<0036:GPAODD>2.0.CO;2.

Huffman, G. J., D. T. Bolvin, E. J. Nelkin, D. B. Wolff, R. F. Adler, G. Gu, Y. Hong, K. P. Bowman, and E. F. Stocker (2007), The TRMM Multisatellite Precipitation Analysis (TMPA): Quasi-global, multiyear, combined-sensor precipitation estimates at fine scales, *J. Hydrometeorol.*, *8*(1), 38–55, doi:10.1175/JHM560.1.

Huffman, G. J., R. F. Adler, D. T. Bolvin, and G. Gu (2009), Improving the global precipitation record: GPCP version 2.1, *Geophys. Res. Lett.*, *36*, L17808, doi:10.1029/2009GL040000.

Huffman, G., R. Adler, D. Bolvin, and E. Nelkin (2010), The TRMM Multi-Satellite Precipitation Analysis (TMPA), in *Satellite Rainfall Applications for Surface Hydrology*, pp. 3–22, Springer, Netherlands.

Hulme, M., R. Doherty, T. Ngara, M. New, and D. Lister (2001), African climate change: 1900-2100, *Clim. Res.*, *17*(2), 145–168.

Intergovernmental Panel on Climate Change (2013), Climate change 2013: The physical science basis, in *Contribution of Working Group I to the Fifth Assessment Report of the Intergovernmental Panel on Climate Change*, edited by T. F. Stocker et al., 1535 pp., Cambridge Univ. Press, Cambridge, U. K., and New York.

Janowiak, J. E. (1988), An investigation of interannual rainfall variability in Africa, *J. Clim.*, *1*(3), 240–255, doi:10.1175/1520-0442(1988)001<0240:AIOIRV>2.0.CO;2.

Jobard, I., F. Chopin, J. C. Berges, and R. Roca (2011), An intercomparison of 10-day satellite precipitation products during West African monsoon, *Int. J. Remote Sens.*, *32*(9), 2353–2376, doi:10.1080/01431161003698286.

Joyce, R., and P. A. Arkin (1997), Improved estimates of tropical and subtropical precipitation using the GOES precipitation index, *J. Atmos. Oceanic Tech.*, *14*(5), 997–1011, doi:10.1175/1520-0426(1997)014<0997:IEOTAS>2.0.CO;2.

Joyce, R. J., J. E. Janowiak, P. A. Arkin, and P. Xie (2004), CMORPH: A method that produces global precipitation estimates from passive microwave and infrared data at high spatial and temporal resolution, *J. Hydrometeorol.*, *5*(3), 487–503.

Kidd, C., and G. Huffman (2011), Global precipitation measurement, *Meteorol. Appl.*, *18*(3), 334–353, doi:10.1002/met.284.

Kidd, C., and V. Levizzani (2011), Status of satellite precipitation retrievals, *Hydrol. Earth Syst. Sci.*, *15*(4), 1109–1116, doi:10.5194/hess-15-1109-2011.

Kidd, C., D. R. Kniveton, M. C. Todd, and T. J. Bellerby (2003), Satellite rainfall estimation using combined passive microwave and infrared algorithms, *J. Hydrometeorol.*, *4*(6), 1088–1104, doi:10.1175/1525-7541(2003)004<1088:SREUCP>2.0.CO;2.

Kucera, P. A., E. E. Ebert, F. J. Turk, V. Levizzani, D. Kirschbaum, F. J. Tapiador, A. Loew, and M. Borsche (2013), Precipitation from space: Advancing Earth system science, *Bull. Am. Meteorol. Soc.*, *94*(3), 365–375, doi:10.1175/BAMS-D-11-00171.1.

Kummerow, C., et al. (2000), The status of the Tropical Rainfall Measuring Mission (TRMM) after Two years in orbit, *J. Appl. Meteorol.*, *39*(12), 1965–1982, doi:10.1175/1520-0450(2001)040<1965:TSOTTR>2.0.CO;2.

Lamb, P. J., and R. A. Peppler (1992), Further case studies of tropical Atlantic surface atmospheric and oceanic patterns associated with sub-Saharan drought, *J. Clim.*, *5*(5), 476–488, doi:10.1175/1520-0442(1992)005<0476:FCSOTA>2.0.CO;2.

Lau, K.-M., and H.-T. Wu (2007), Detecting trends in tropical rainfall characteristics, 1979–2003, *Int. J. Climatol.*, *27*(8), 979–988, doi:10.1002/joc.1454.

Laurent, H., I. Jobard, and A. Toma (1998), Validation of satellite and ground-based estimates of precipitation over the Sahel, *Atmos. Res.*, *47*, 651–670.

Legates, D. R., and C. J. Willmott (1990), Mean seasonal and spatial variability in gauge-corrected, global precipitation, *Int. J. Climatol.*, *10*(2), 111–127, doi:10.1002/joc.3370100202.

Lim, H.-S., and C.-H. Ho (2000), Comparison of tropical rainfall between the observed GPCP data and the assimilation products of ECMWF, NCEP/NCAR, and NASA-GEOS-1, *J. Meteorol. Soc. Jpn.*, *78*(5), 661–672.

Liu, C., and E. J. Zipser (2009), "Warm rain" in the tropics: Seasonal and regional distributions based on 9 yr of TRMM data, *J. Clim.*, *22*(3), 767–779, doi:10.1175/2008JCLI2641.1.

Love, T. B., V. Kumar, P. Xie, and W. Thiaw (2004), A 20-year daily Africa precipitation climatology using satellite and gauge data, in *American Meteorological Society Conference on Applied Climatology*, Seattle, Wash.

Maidment, R. I., D. I. F. Grimes, R. P. Allan, H. Greatrex, O. Rojas, and O. Leo (2013), Evaluation of satellite-based and model re-analysis rainfall estimates for Uganda, *Meteorol. Appl.*, *20*(3), 308–317, doi:10.1002/met.1283.

Mathon, V., H. Laurent, and T. Lebel (2002), Mesoscale convective system rainfall in the Sahel, *J. Appl. Meteorol.*, *41*(11), 1081–1092, doi:10.1175/1520-0450(2002)041<1081:MCSRIT>2.0.CO;2.

Menne, M. J., I. Durre, R. S. Vose, B. E. Gleason, and T. G. Houston (2012), An overview of the global historical climatology network-daily database, *J. Atmos. Oceanic Tech.*, *29*(7), 897–910, doi:10.1175/JTECH-D-11-00103.1.

Milford, J. R., V. D. McDougall, and G. Dugdale (1996), Rainfall estimation from cold cloud duration: Experience of the TAMSAT group in West Africa, in *Colloques et Seminaires*. *Validation Problems of Rainfall Estimation Methods by Satellite in Intertropical Africa*. *Proceedings of the Niamey Workshop* (*1994*), ORSTROM.

Mitchell, T. D., and P. D. Jones (2005), An improved method of constructing a database of monthly climate observations and associated high-resolution grids, *Int. J. Climatol.*, *25*(6), 693–712, doi:10.1002/joc.1181.

Mohr, K., and E. Zipser (1996), Mesoscale convective systems defined by their 85-GHz ice scattering signature: Size and intensity comparison over tropical oceans and continents, *Mon. Weather Rev.*, *124*, 2417–2437.

Mohr, K. I., J. S. Famiglietti, and E. J. Zipser (1999), The contribution to tropical rainfall with respect to convective system type, size, and intensity estimated from the 85-GHz Ice-scattering signature, *J. Appl. Meteorol.*, *38*(5), 596–606, doi:10.1175/1520-0450(1999)038<0596:TCTTRW>2.0.CO;2.

Nesbitt, S., E. Zipser, and D. Cecil (2000), A census of precipitation features in the tropics using TRMM: Radar, ice scattering, and lightning observations, *J. Clim.*, *13*, 4087–4106.

Nicholson, S. E. (2001), Climatic and environmental change in Africa during the last two centuries, *Clim. Res.*, *17*(2), 123–144.

Nicholson, S. E., and J. C. Selato (2000), The influence of La Nina on African rainfall, *Int. J. Climatol.*, *20*(14), 1761–1776, doi:10.1002/1097-0088(20001130)20:14<1761::AID-JOC580>3.0.CO;2-W.

Nicholson, S. E., et al. (2003a), Validation of TRMM and other rainfall estimates with a high-density gauge dataset for West Africa. Part I: Validation of GPCC rainfall product and pre-TRMM satellite and blended products, *J. Appl. Meteorol.*, *42*(10), 1337–1354, doi:10.1175/1520-0450(2003)042<1337:VOTAOR>2.0.CO;2.

Nicholson, S. E., et al. (2003b), Validation of TRMM and other rainfall estimates with a high-density gauge dataset for West Africa. Part II: Validation of TRMM rainfall products, *J. Appl. Meteorol.*, *42*(10), 1355–1368, doi:10.1175/1520-0450(2003)042<1355:VOTAOR>2.0.CO;2.

Novella, N. S., and W. M. Thiaw (2013), African rainfall climatology version 2 for famine early warning systems, *J. Appl. Meteorol. Climatol.*, *52*(3), 588–606, doi:10.1175/JAMC-D-11-0238.1.

Pearson, K. J., G. M. S. Lister, C. E. Birch, R. P. Allan, R. J. Hogan, and S. J. Woolnough (2014), Modelling the diurnal cycle of tropical convection across the "grey zone", *Q. J. R. Meteorol. Soc.*, *140*(679), 491–499, doi:10.1002/qj.2145.

Picon, L., R. Roca, S. Serrar, J. L. Monge, and M. Desbois (2003), A new METEOSAT "water vapor" archive for climate studies, *J. Geophys. Res.*, *108*(D10), 4301, doi:10.1029/2002JD002640.

Poccard, I., S. Janicot, and P. Camberlin (2000), Comparison of rainfall structures between NCEP/NCAR reanalyses and observed data over tropical Africa, *Clim. Dyn.*, *16*(12), 897–915, doi:10.1007/s003820000087.

Pope, V. D., M. L. Gallani, P. R. Rowntree, and R. A. Stratton (2000), The impact of new physical parametrizations in the Hadley Centre climate model: HadAM3, *Clim. Dyn.*, *16*(2–3), 123–146, doi:10.1007/s003820050009.

Reynolds, R. (1988), A real-time global sea surface temperature analysis, *J. Clim.*, *1*, 75–87.

Roca, R., P. Chambon, I. Jobard, P.-E. Kirstetter, M. Gosset, and J. C. Bergès (2010), Comparing satellite and surface rainfall products over West Africa at meteorologically relevant scales during the AMMA campaign using error estimates, *J. Appl. Meteorol. Climatol.*, *49*(4), 715–731, doi:10.1175/2009JAMC2318.1.

Roebeling, R. A., E. L. A. Wolters, J. F. Meirink, and H. Leijnse (2012), Triple collocation of summer precipitation retrievals from SEVIRI over Europe with gridded rain gauge and weather radar data, *J. Hydrometeorol.*, *13*(5), 1552–1566, doi:10.1175/JHM-D-11-089.1.

Roebeling, R., J. Schulz, T. Hewison, and B. Theodore (2013), Inter-calibration of METEOSAT IR and WV channels using HIRS, *AIP Conf. Proc.*, *288*, 288–291, doi:10.1063/1.4804763.

Rossow, W., and R. Schiffer (1999), Advances in understanding clouds from ISCCP, *Bull. Am. Meteorol. Soc.*, *80*(11), 2261–2287.

Rudolf, B., H. Hauschild, W. Rueth, and U. Schneider (1994), Terrestrial precipitation analysis: Operational method and required density of point measurements, *Glob. Precip. Clim. Chang.*, *26*, 173–186.

Schiffer, R., and W. Rossow (1985), ISCCP global radiance data set: A new resource for climate research, *Bull. Am. Meteorol. Soc.*, *66*(12), 1498–1505.

Schneider, U., A. Becker, P. Finger, A. Meyer-Christoffer, M. Ziese, and B. Rudolf (2014), GPCC's new land surface precipitation climatology based on quality-controlled in situ data and its role in quantifying the global water cycle, *Theor. Appl. Climatol.*, *115*(1–2), 15–40, doi:10.1007/s00704-013-0860-x.

Schumacher, C., and R. Houze (2003), The TRMM precipitation radar's view of shallow, isolated rain, *J. Appl. Meteorol.*, *42*, 1519–1524.

Schumacher, C., and R. A. Houze (2006), Stratiform precipitation production over sub-Saharan Africa and the tropical East Atlantic as observed by TRMM, *Q. J. R. Meteorol. Soc.*, *132*(620), 2235–2255, doi:10.1256/qj.05.121.

Sealy, A., G. S. Jenkins, and S. C. Walford (2003), Seasonal/regional comparisons of rain rates and rain characteristics in West Africa using TRMM observations, *J. Geophys. Res.*, *108*(D10), 4306, doi:10.1029/2002JD002667.

Sevruk, B. (1982), Methods of correction for systematic error in point precipitation measurements for operational use, in *WMO Operational Hydrology Report 21*.

Tarnavsky, E., D. Grimes, R. I. Maidment, M. Stringer, R. Chadwick, R. P. Allan, E. Black, and F. Kayitakire (2014), Extension of the TAMSAT Satellite-based Rainfall Monitoring over Africa and from 1983 to present, *J. Appl. Meteorol. Climatol.*, doi:10.1175/JAMC-D-14-0016.1.

Thiemig, V., R. Rojas, M. Zambrano-Bigiarini, V. Levizzani, and A. De Roo (2012), Validation of satellite-based precipitation products over sparsely gauged African river basins, *J. Hydrometeorol.*, *13*(6), 1760–1783, doi:10.1175/JHM-D-12-032.1.

Thorne, V., P. Coakeley, D. Grimes, and G. Dugdale (2001), Comparison of TAMSAT and CPC rainfall estimates with raingauges, for southern Africa, *Int. J. Remote Sens.*, *22*(10), 1951–1974, doi:10.1080/01431160118816.

Todd, M. C., E. C. Barrett, M. J. Beaumont, and J. L. Green (1995), Satellite identification of rain days over the upper Nile river basin using an optimum infrared rain/no-rain threshold temperature model, *J. Appl. Meteorol.*, *34*(12), 2600–2611, doi:10.1175/1520-0450(1995)034<2600:SIORDO>2.0.CO;2.

Todd, M. C., E. C. Barrett, M. J. Beaumont, and T. J. Bellerby (1999), Estimation of daily rainfall over the upper Nile river basin using a continuously calibrated satellite infrared technique, *Meteorol. Appl.*, *6*(3), 201–210, doi:10.1017/S1350482799001206.

Trenberth, K. E. et al. (2007), Observations: Surface and atmospheric climate change, in *Climate Change 2007: The Physical Science Basis. Contribution of Working Group I to the Fourth Assessment Report of the Intergovernmental Panel on Climate Change*, edited by S. Solomon et al., Cambridge Univ. Press, Cambridge, U. K., and New York.

Van de Berg, L. C. J., J. Schmetz, and J. Whitlock (1995), On the calibration of the Meteosat water vapor channel, *J. Geophys. Res.*, *100*(D10), 21,069–21,076, doi:10.1029/95JD01880.

Verdin, J., C. Funk, G. Senay, and R. Choularton (2005), Climate science and famine early warning, *Philos. Trans. R. Soc. London, Ser. B*, *360*(1463), 2155–2168, doi:10.1098/rstb.2005.1754.

Wan, H., X. Zhang, F. W. Zwiers, and H. Shiogama (2013), Effect of data coverage on the estimation of mean and variability of precipitation at global and regional scales, *J. Geophys. Res. Atmos.*, *118*, 534–546, doi:10.1002/jgrd.50118.

Washington, R., G. Kay, M. Harrison, D. Conway, E. Black, A. Challinor, D. Grimes, R. Jones, A. Morse, and M. Todd (2006), African climate change: Taking the shorter route, *Bull. Am. Meteorol. Soc.*, *87*(10), 1355–1366, doi:10.1175/BAMS-87-10-1355.

Willmott, C. J., S. M. Robeson, and J. J. Feddema (1994), Estimating continental and terrestrial precipitation averages from rain-gauge networks, *Int. J. Climatol.*, *14*(4), 403–414, doi:10.1002/joc.3370140405.

Xie, P., and P. A. Arkin (1995), An intercomparison of gauge observations and satellite estimates of monthly precipitation, *J. Appl. Meteorol.*, *34*(5), 1143–1160, doi:10.1175/1520-0450(1995)034<1143:AIOGOA>2.0.CO;2.

Xie, P., and P. A. Arkin (1997), Global precipitation: A 17-year monthly analysis based on gauge observations, satellite estimates, and numerical model outputs, *Bull. Am. Meteorol. Soc.*, *78*(11), 2539–2558.

Yang, G., and J. Slingo (2001), The diurnal cycle in the tropics, *Mon. Weather Rev.*, *129*, 784–801.

Yin, X., and A. Gruber (2010), Validation of the abrupt change in GPCP precipitation in the Congo River Basin, *Int. J. Climatol.*, *30*(1), 110–119, doi:10.1002/joc.1875.

Yin, X., A. Gruber, and P. Arkin (2004), Comparison of the GPCP and CMAP merged gauge–satellite monthly precipitation products for the period 1979–2001, *J. Hydrometeorol.*, *5*(6), 1207–1222, doi:10.1175/JHM-392.1.

Zelinka, M. D., and D. L. Hartmann (2011), The observed sensitivity of high clouds to mean surface temperature anomalies in the tropics, *J. Geophys. Res.*, *116*, D23103, doi:10.1029/2011JD016459.